

RESEARCH ARTICLE

# *Plasmodium* P-Type Cyclin CYC3 Modulates Endomitotic Growth during Oocyst Development in Mosquitoes

Magali Roques<sup>1</sup>✉, Richard J. Wall<sup>1</sup>✉<sup>aa</sup>, Alexander P. Douglass<sup>1</sup>✉<sup>ab</sup>, Abhinay Ramaprasad<sup>2</sup>✉, David J. P. Ferguson<sup>3</sup>, Mbinda L. Kaindama<sup>1</sup>, Lorenzo Brusini<sup>1</sup>, Nimitray Joshi<sup>1</sup>, Zineb Rchiad<sup>2</sup>, Declan Brady<sup>1</sup>, David S. Guttery<sup>1</sup>✉<sup>ac</sup>, Sally P. Wheatley<sup>1</sup>, Hiroyuki Yamano<sup>4</sup>, Anthony A. Holder<sup>5</sup>, Arnab Pain<sup>2</sup>✉<sup>ad</sup>, Bill Wickstead<sup>1</sup>\*, Rita Tewari<sup>1</sup>\*

**1** School of Life Sciences, Queens Medical Centre, University of Nottingham, Nottingham, United Kingdom, **2** Biological and Environmental Sciences and Engineering (BESE) Division, King Abdullah University of Science and Technology, Thuwal, Kingdom of Saudi Arabia, **3** Nuffield Department of Clinical Laboratory Science, University of Oxford, John Radcliffe Hospital, Oxford, United Kingdom, **4** UCL Cancer Institute, University College London, London, United Kingdom, **5** Mill Hill Laboratory, The Francis Crick Institute, Mill Hill, London, United Kingdom

✉ These authors contributed equally to this work.

<sup>aa</sup> Current Address: Division of Biological Chemistry and Drug Discovery, School of Life Sciences, University of Dundee, Dundee, United Kingdom

<sup>ab</sup> Current Address: Conway Institute, University College Dublin, Dublin 4, Republic of Ireland

<sup>ac</sup> Current Address: Department of Cancer Studies, University of Leicester, Robert Kilpatrick Building, PO Box 65, Leicester Royal Infirmary, Leicester, United Kingdom

<sup>ad</sup> Current Address: Center for Zoonosis Control, Global Institution for Collaborative Research and Education (GI-CoRE), Hokkaido University, N20 W10 Kita-ku, Sapporo, 001–0020 Japan

\* [bill.wickstead@nottingham.ac.uk](mailto:bill.wickstead@nottingham.ac.uk) (BW); [rita.tewari@nottingham.ac.uk](mailto:rita.tewari@nottingham.ac.uk) (RT)



**OPEN ACCESS**

**Citation:** Roques M, Wall RJ, Douglass AP, Ramaprasad A, Ferguson DJP, Kaindama ML, et al. (2015) *Plasmodium* P-Type Cyclin CYC3 Modulates Endomitotic Growth during Oocyst Development in Mosquitoes. PLoS Pathog 11(11): e1005273. doi:10.1371/journal.ppat.1005273

**Editor:** Kami Kim, Albert Einstein College of Medicine, UNITED STATES

**Received:** August 15, 2015

**Accepted:** October 21, 2015

**Published:** November 13, 2015

**Copyright:** © 2015 Roques et al. This is an open access article distributed under the terms of the [Creative Commons Attribution License](https://creativecommons.org/licenses/by/4.0/), which permits unrestricted use, distribution, and reproduction in any medium, provided the original author and source are credited.

**Data Availability Statement:** All relevant data are within the paper and its Supporting Information files.

**Funding:** AAH is supported by the Francis Crick Institute which receives its core funding from Cancer Research UK, the UK Medical Research Council, and the Wellcome Trust. Work in the HY laboratory was funded by grants from Cancer Research UK (C8320/A13586) and MRC (MR/M010899/1). Part of the work done in AP laboratory was supported by the faculty baseline funding and a CRG3 grant from King Abdullah University of Science and Technology (KAUST). Imaging was performed by SPW in the

## Abstract

Cell-cycle progression and cell division in eukaryotes are governed in part by the cyclin family and their regulation of cyclin-dependent kinases (CDKs). Cyclins are very well characterised in model systems such as yeast and human cells, but surprisingly little is known about their number and role in *Plasmodium*, the unicellular protozoan parasite that causes malaria. Malaria parasite cell division and proliferation differs from that of many eukaryotes. During its life cycle it undergoes two types of mitosis: endomitosis in asexual stages and an extremely rapid mitotic process during male gametogenesis. Both schizogony (producing merozoites) in host liver and red blood cells, and sporogony (producing sporozoites) in the mosquito vector, are endomitotic with repeated nuclear replication, without chromosome condensation, before cell division. The role of specific cyclins during *Plasmodium* cell proliferation was unknown. We show here that the *Plasmodium* genome contains only three cyclin genes, representing an unusual repertoire of cyclin classes. Expression and reverse genetic analyses of the single Plant (P)-type cyclin, CYC3, in the rodent malaria parasite, *Plasmodium berghei*, revealed a cytoplasmic and nuclear location of the GFP-tagged protein throughout the lifecycle. Deletion of *cyc3* resulted in defects in size, number and growth of oocysts, with abnormalities in budding and sporozoite formation. Furthermore, global transcript analysis of the *cyc3*-deleted and wild type parasites at gametocyte and ookinete stages identified differentially expressed genes required for signalling, invasion and oocyst

Advanced Microscopy Unit, at the University of Nottingham with a DeltaVision Elite system funded by the Wellcome Trust (WT094233MA). This project was funded by MRC Investigator Award and MRC project grants to RT [G0900109, G0900278, MR/K011782/1] and a BBSRC new investigator research grant to BW [BB/J01477X/1]. The funders had no role in study design, data collection and analysis, decision to publish, or preparation of the manuscript.

**Competing Interests:** The authors have declared that no competing interests exist.

development. Collectively these data suggest that *cyc3* modulates oocyst endomitotic development in *Plasmodium berghei*.

## Author Summary

The malaria parasite is a single-celled organism that multiplies asexually in a non-canonical way in both vertebrate host and mosquito vector. In the mosquito midgut, atypical cell division occurs in oocysts, where repeated nuclear division (endomitosis) precedes cell division, which then gives rise to many sporozoites in a process known as sporogony. The molecular mechanisms controlling this process are poorly understood. In many model organisms including mouse and yeast cells the cell cycle is regulated by members of the cyclin protein family, but the role of this family in the malaria parasite is unknown. Here, we show that there are only three cyclin genes and investigate the function of the single P-type cyclin (CYC3) in the rodent malaria parasite, *Plasmodium berghei*. We show that CYC3 has a cytoplasmic and nuclear localisation throughout most of the parasite lifecycle and by gene deletion we demonstrate that CYC3 is important for normal oocyst development, maturation and sporozoite formation. Moreover, we show that deletion of *cyc3* affects the transcription of genes required for cell signalling and oocyst development. The data suggest that CYC3 modulates asexual multiplication in oocysts and plays a vital role in parasite development in the mosquito.

## Introduction

The mechanisms of mitotic cell division and the various molecules involved are well studied in many model systems including yeast, plants and human cells. Progression through mitosis is controlled by a range of factors, including cyclins, protein kinases (PKs) and phosphatases (PPs), and the anaphase-promoting complex (APC) components [1–4]. Cyclins play active roles at distinct stages of the cell cycle [4] via regulation of cyclin-dependent kinases (CDKs). Cyclins possess a conserved ~100-residue sequence known as the cyclin box that mediates CDK binding and activation [5]. Certain cyclins are capable of binding several CDKs, which are themselves able to associate with multiple cyclins [6,7]. These distinct but overlapping functions orchestrate cell cycle progression.

In most model systems, the synthesis and level of cyclins are tightly regulated during the cell cycle, with each cyclin being degraded via ubiquitination once its function is complete [8,9]. Key cell cycle transitions are regulated by specific cyclins: G1/S cyclins, which are essential for cell cycle entry at G1/S (start), and G2/M cyclins, which are essential at the G2/M (mitosis) transition. In some species, there are multiple forms of G1 and G2 cyclins. For example, in vertebrates there are at least three G1 cyclins (C, D, and E) and two G2 cyclins (A, which is also active in S phase, and B). Many other cyclins with additional functions have also been described [10,11].

Recent bioinformatic analyses have identified 3 distinct classes of cyclin: Group I (including cyclin A, B, D, E, F, G, I, J, and O families), Group II (P/Pho80-like, and Y), and Group III (C, H, K, L, and T) [12,13]. Group I includes known essential cell cycle cyclins including some involved in mitosis and meiosis [10,14,15], while Group III contains cyclins associated with transcription and RNA processing [11]. Group II contains both cell cycle cyclins and those of other function, such as cell metabolism (e.g. P-type cyclins (CYCPs), which were originally

believed to be unique to plants) and appear to link cell cycle regulation to nutritional status [16–18]. The cyclin box of CYCP in plants shows high similarity to the corresponding domain of trypanosome cyclins CYC2, CYC4, CYC7, CYC10 and CYC11 [13,19] and *S. cerevisiae* PHO80-like cyclins [20].

Malaria parasites, *Plasmodium*, which belong to the phylum *Apicomplexa*, divide and proliferate in an unusual way compared to other eukaryotes. During its life cycle, *Plasmodium* exhibits two types of cell division; one in asexual stages that resembles endomitosis and one in sexual stages. The endomitotic-like asexual stage is characterized by multiple nuclear divisions preceding cytokinesis, with maintenance of the nuclear membrane wherein the microtubule organising centre (MTOC) or spindle body is embedded [21–23]. This process is observed at three developmental stages of the parasite life cycle: during schizogony, replication and multiplication within liver and red blood cells in the vertebrate host [21], and at the sporogonic stage of parasite development in the mosquito vector [24]. The other type of cell division occurs during male gametogenesis, where three rounds of rapid DNA replication are followed by cell division and chromosome condensation giving rise to eight microgametes [23,25,26].

In the human malaria parasite, *Plasmodium falciparum*, the stages of development during asexual multiplication inside red blood cells have been described as (a) ring stage (early trophozoite) with a single (haploid) interphase nucleus in G<sub>0</sub>, (b) mature trophozoites ready for chromosome replication (G<sub>1</sub>) and undergoing DNA synthesis (S phase), and (c) the schizont stage when asynchronous nuclear division begins (M phase) and repeated S and M phases continue resulting in a multinucleate syncytium [21,27]. At the end of the growth phase, cell division occurs in the late stage schizont or segmenter to form merozoites that are released to invade new red blood cells. This process resembles that of endomitosis observed in *Drosophila* cells [28].

The molecular mechanisms that regulate nuclear and cell division in the malaria parasite remain largely unknown. We have previously shown that the single putative homologue of cell division cycle protein 20 (CDC20), a well-characterised activator of the anaphase promoting complex/cyclosome (APC/C), is crucial for karyokinesis and cytokinetic control of male gametogenesis [29]. Furthermore, systematic genome-wide functional analysis of the protein kinome and phosphatome has identified molecules crucial for both male gametogenesis and asexual multiplication during sporogony, including CDKs, CDPK4, MAP2 and PTPLA [30–32]. *Plasmodium* has a number of genes that code for calcium dependent protein kinases (CDPKs) that are implicated in control of growth and cell division [31,32]. Other kinases, such as ARK1, an aurora-like kinase associated with the spindle pole body, have been identified and implicated in cell division [33]. Knowledge of cyclin function in *Plasmodium* is limited. Previously, four cyclin genes were described in *P. falciparum*, *Pfcyc1* to *-4* [34,35]. Biochemical studies showed that *PfCYC1*, *PfCYC3* and *PfCYC4* associate with histone H1 kinase activity present in the parasite extract [35], and *PfCYC1* and *PfCYC3* bind and activate the *Plasmodium* CDK1 homologue (PK5) *in vitro* [34,35]. *PfPK5* has also been shown to be activated by mammalian proteins (p25 and RINGO) that have no detectable primary sequence similarity to cyclin [34,35]. Recently, *PbCYC3* has been shown to be a target gene of the AP2-O transcription factor, and is involved in oocyst development [36].

Here, we describe an in-depth phylogenetic analysis of the cyclin repertoire in *Plasmodium*. We then focus on the single P-type cyclin (CYC3) and examine its role during parasite cell division, using the rodent malaria model *Plasmodium berghei*. We show that whilst CYC3 is dispensable for asexual cell cycle progression in the mammalian host, it modulates oocyst development and the subsequent differentiation of sporozoites, the endomitotic process of sporogony within the mosquito vector.

## Results

### *Plasmodium* parasites have a small, unusual complement of cyclins

Cyclins are a diverse superfamily of proteins (for example see [13]). A number of PFam models incorporate parts of the conserved domain (including PF08613, PF00134, PF02984), but none covers the entire conserved region and each is biased towards particular classes.

To investigate the *Plasmodium* cyclin repertoire, we built a pan-cyclin hidden Markov model (HMM) of cyclins from a range of model species and used this to identify putative cyclins in a wide range of eukaryotes (see [Methods](#)). Our HMM showed good sensitivity, identifying full cyclin repertoires in diverse organisms not included in the seed alignment, and the resultant protein sequences were aligned, trimmed to conserved regions and classified by constructing phylogenetic trees ([Fig 1A](#) and [S1 Fig](#)).

*Plasmodium* species encode only three identifiable cyclins—CYC1, CYC3 and CYC4. A *P. falciparum* gene (encoded by PF3D7\_1227500) annotated as *PfCYC2* did not show a significant match to any of the cyclin-specific HMMs built during these analyses (even at extremely liberal thresholds), nor to the domains built by PFam. This protein was originally identified as a cyclin on the basis of a very limited similarity to a cyclin A from the sea star *Patiria (Asterina) pectinifera* (13% identity across alignable length) [35], but it lacks key alignable residues across most of the cyclin box and has no detectable cyclin-like function in biochemical assays [35]. These data strongly suggest that CYC2 is not a true cyclin and it is not included in the repertoire described here.

The *Plasmodium* cyclin repertoire is highly unusual in that it entirely lacks Group I, the largest group of cyclins. This group contains most canonical cyclin families that regulate specific cell cycle transitions with their CDK partners: Cyclin D-CDK4/6 for G1 progression, Cyclin E-CDK2 for the G1/S transition, Cyclin A-CDK2 for S phase progression and Cyclin A/B-CDK1 for mitosis, although in fission yeast, all cell cycle transitions are driven by a single Cyclin B/CDK complex (CDC13/CDC2) [3,37]. In keeping with this key role and previous analyses [13], Group I cyclins were found in all non-apicomplexan species examined here, including the alveolate *Tetrahymena thermophila* [13]. However, none of the apicomplexan species examined contained Group I cyclins, except *Cryptosporidium*, which was found to encode three Group I cyclins of indeterminate family, suggesting that there has been a loss of Group I cyclins during the evolution of apicomplexan lineages ([Fig 1B](#)).

*Plasmodium* species encode only one cyclin from the P family (Group II) and two Group III cyclins from families H and L. The cyclin P family is not found in animals, but includes many plant cyclins and Pho80 in budding yeast, which link nutritional sensing to cell cycle progression. In contrast, both H and L families are associated with transcription: the CDK7/Cyclin H/MAT1 complex functions as a Cdk-activating kinase in cell cycle regulation [38] and as a modulator of the general transcription factor TFIIF [39,40]. Similarly, CDK11-Cyclin L complex in fission yeast regulates the formation of the Mediator complex, a coactivator of RNA polymerase II transcription [41].

### *Plasmodium* cyclins are transcribed at all developmental stages

We used quantitative RT-PCR (qRT-PCR) to investigate the RNA levels of *cyc1*, 3 and 4 in six stages of the wild-type parasite life cycle. The transcription profiles showed expression of the cyclins throughout parasite development with the highest RNA levels for all three cyclins found in gametocytes (both non-activated and activated) and schizonts (particularly *cyc4*). The *cyc3* RNA level was highest in non-activated gametocytes, whereas for *cyc1* and *cyc4*, the levels were highest in activated gametocytes ([Fig 2A](#)). These results are similar to those obtained

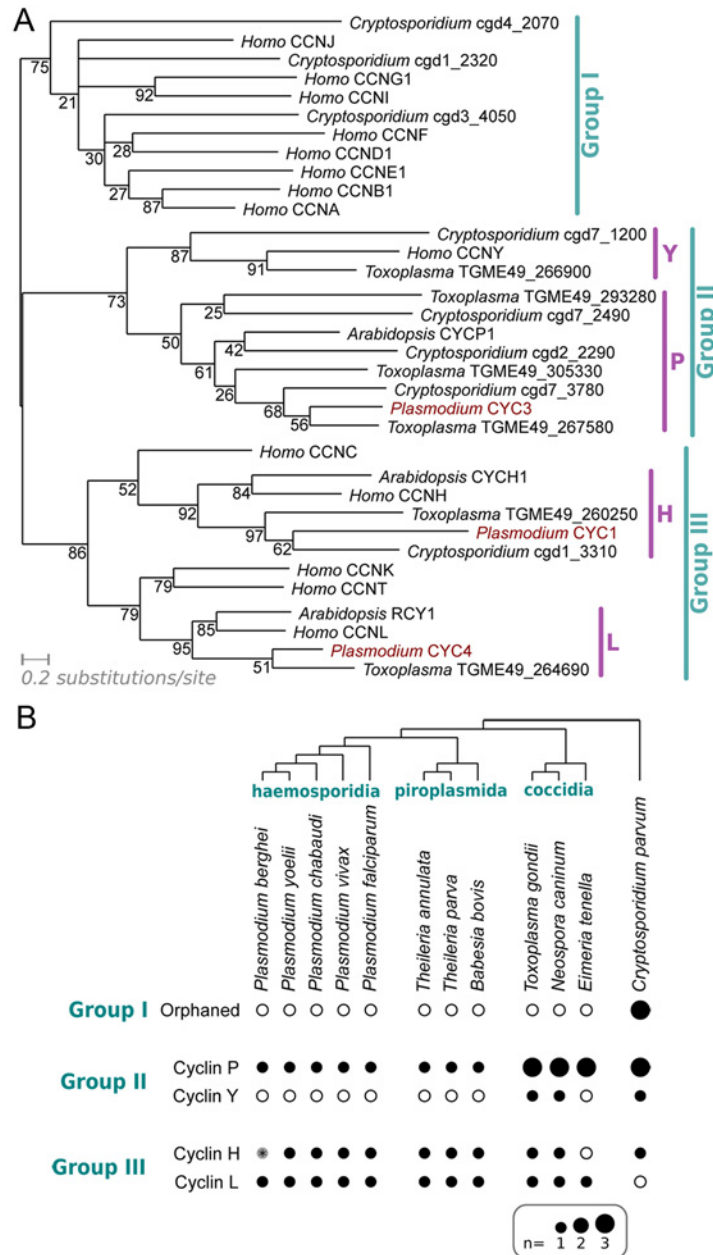


**Fig 1. Characterisation of the cyclin repertoire of the Apicomplexa.** (A) Maximum likelihood phylogeny based on an alignment of cyclins from *Plasmodium falciparum*, *Toxoplasma gondii*, *Cryptosporidium parvum* and *Homo sapiens*. CYCP1 and CYCH1 from *Arabidopsis thaliana* have been included for clarity. Topology support from bootstrapping is shown at nodes. (B) Distribution of cyclin families across Apicomplexa. Presence (filled dot) or absence (empty circle) of specific families of cyclin in each predicted proteome is shown. Dot area is proportional to number of putative proteins. The Group I cyclins in *Cryptosporidium* cannot be placed reliably into any specific families within the group (“Orphaned”). \*The *Plasmodium berghei* predicted proteome (release 9.3; plasmodb.org) contains no apparent orthologue of CYC1, as the likely gene encoding the protein on Chromosome 13 (downstream of PBANKA\_132730, syntenic with *cyc1* in other *Plasmodium* species) is interrupted by a sequence gap.

doi:10.1371/journal.ppat.1005273.g001

previously for *P. berghei* by RNA-seq analysis [42] and for *P. falciparum* using both RT-PCR [35] and RNA-seq [43].

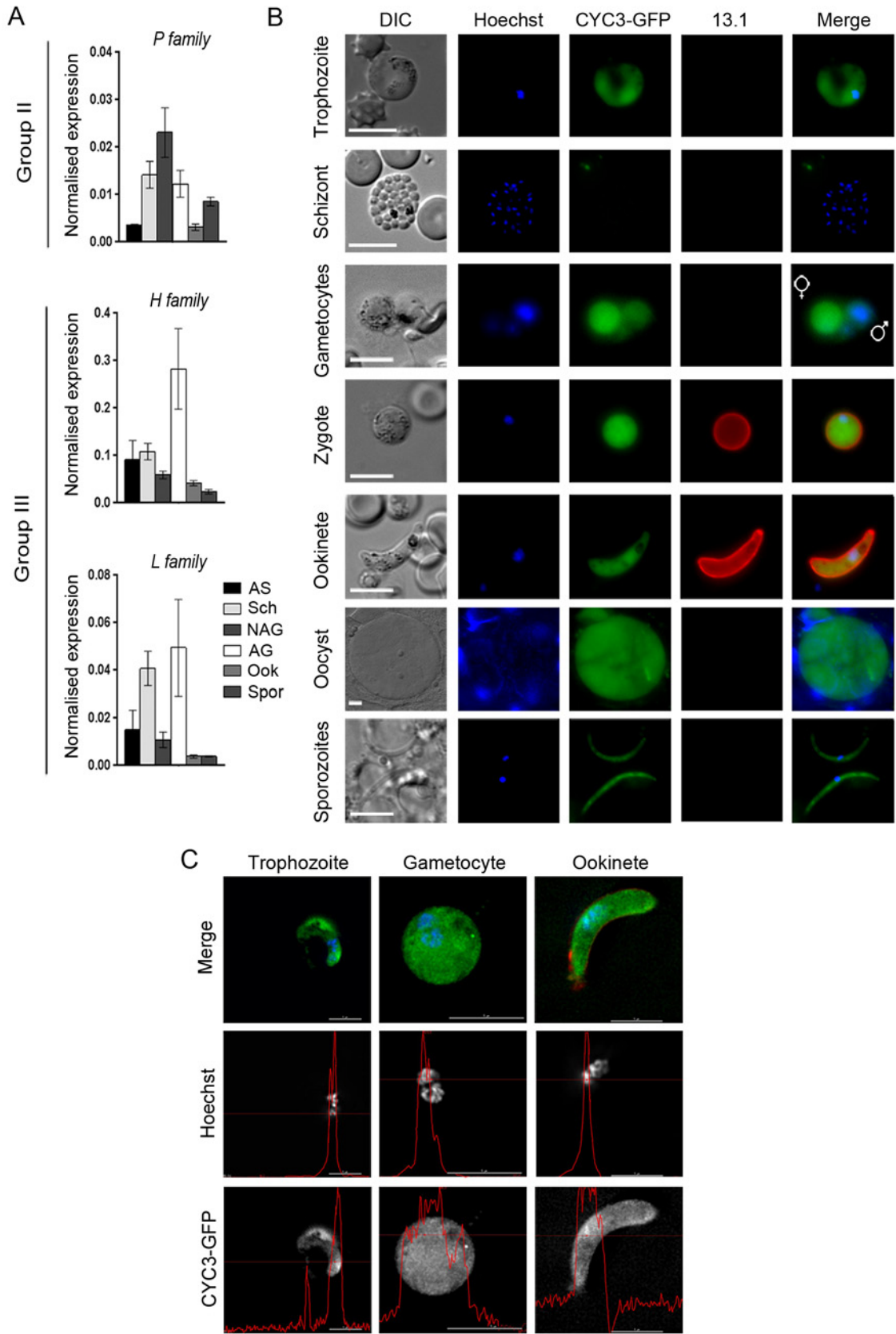


**Fig 2. CYC3-GFP protein expression throughout most stages of the life cycle.** (A) Transcription of *cyc1*, *cyc3* and *cyc4* as analysed by qRT-PCR, normalised against two endogenous control genes, *arginine-tRNA synthetase* and *hsp70*. Each bar is the mean of three biological replicates  $\pm$  SEM. All asexual blood stages: AS; schizonts: Sch; non-activated gametocytes: NAG; activated gametocytes: AG; ookinete: Ook; 14 dpi oocysts/sporozoites: Spor. (B) Expression of CYC3-GFP in trophozoites, schizonts, gametocytes, zygotes, ookinetes, oocysts and sporozoites. 13.1, a cy3-conjugated antibody which recognises P28 on the surface of activated females, zygotes, and ookinetes was used with the sexual stages. Scale bar = 5  $\mu$ m. (C) Deconvolved 2D projections of live trophozoite, gametocyte, and ookinete expressing CYC3-GFP (green), co-stained with Hoechst 33342 (blue) and cy3-conjugated anti-P28 antibody, 13.1 as a marker for the ookinete surface (red). Scale bar = 5  $\mu$ m. Line profiles (red) in the black and white images indicate pixel intensity for that channel.

doi:10.1371/journal.ppat.1005273.g002

## P-type CYC3-GFP is cytosolic and nuclear at most stages of the lifecycle

To investigate the localisation of CYC3, the only P-type cyclin in *Plasmodium*, throughout the *P. berghei* life cycle, we generated a C-terminal GFP fusion protein using single crossover recombination at the endogenous *cyc3* gene locus (PBANKA\_123320; [S2A Fig](#)). Correct integration was confirmed by PCR, pulsed-field gel electrophoresis (PFGE) and Southern blot ([S2B–S2D Fig](#)). CYC3-GFP parasites were able to complete the full life cycle with no detectable phenotype observed from tagging with GFP including oocyst development at 14 days post infection (dpi) in mosquitoes ([S2F and S2G Fig](#)). Western blot with an anti-GFP antibody confirmed the expression of CYC3-GFP. A 54 kDa protein was detected in lysates from three stages of parasite development (schizonts, activated gametocytes and ookinetes) with the highest expression observed in activated gametocyte and ookinete stages compared with the 29 kDa GFP control extracted from a parasite line constitutively expressing GFP (GFPcon 507 cl1) [[44](#)] ([S2E Fig](#)).

Live imaging of parasites revealed CYC3-GFP presence throughout the parasite cell body with a predominantly cytosolic localisation at most of the key *Plasmodium* life cycle stages examined (trophozoite, male and female gametocyte, zygote, ookinete, oocyst and salivary gland sporozoite) ([Fig 2B](#)). However, we could not exclude the presence of CYC3-GFP also in the nucleus of trophozoites, gametocytes and ookinetes ([Fig 2B](#)). Therefore, for a more detailed analysis of the CYC3 localisation at trophozoite, schizont, gametocyte and ookinete stages, we used deconvolution fluorescence imaging ([Fig 2C](#)). Although no expression was detected in schizonts, two dimensional optical slices from 3D stacks showed that CYC3-GFP was uniformly present throughout both the cytoplasm and the nucleus in trophozoites, gametocytes and ookinetes ([Fig 2C](#)) and noticeably enriched in the nucleus of ookinetes ([Fig 2C](#), line profile).

## CYC3 affects oocyst development, differentiation and sporozoite formation within the mosquito

To assess the function of CYC3 in the *Plasmodium* life cycle, we used a double crossover homologous recombination strategy to delete the *cyc3* gene ([S3A Fig](#)). Successful integration of the targeting construct at the *cyc3* locus was confirmed by diagnostic PCR across the junction of the expected integration site, as well as by Southern blot and PFGE ([S3B–S3D Fig](#)).

Analysis of two independent *cyc3* deletion clones, *cyc3* cl1 and *cyc3* cl3 (hence forward called  $\Delta$ *cyc3*) showed no overt phenotype during blood stage asexual proliferation, microgamete exflagellation or ookinete conversion *in vitro* when compared with control parasites which constitutively express untagged GFP (WTGFPcon 507 cl1 line, henceforth known as WT) [[44](#)] ([Fig 3A–3C](#)).

To determine whether CYC3 is essential for parasite development in the mosquito vector, we fed female *Anopheles stephensi* mosquitoes with the  $\Delta$ *cyc3* mutant or WT parasites. There was no significant reduction in the number of  $\Delta$ *cyc3* oocysts compared to WT controls at 5 dpi,

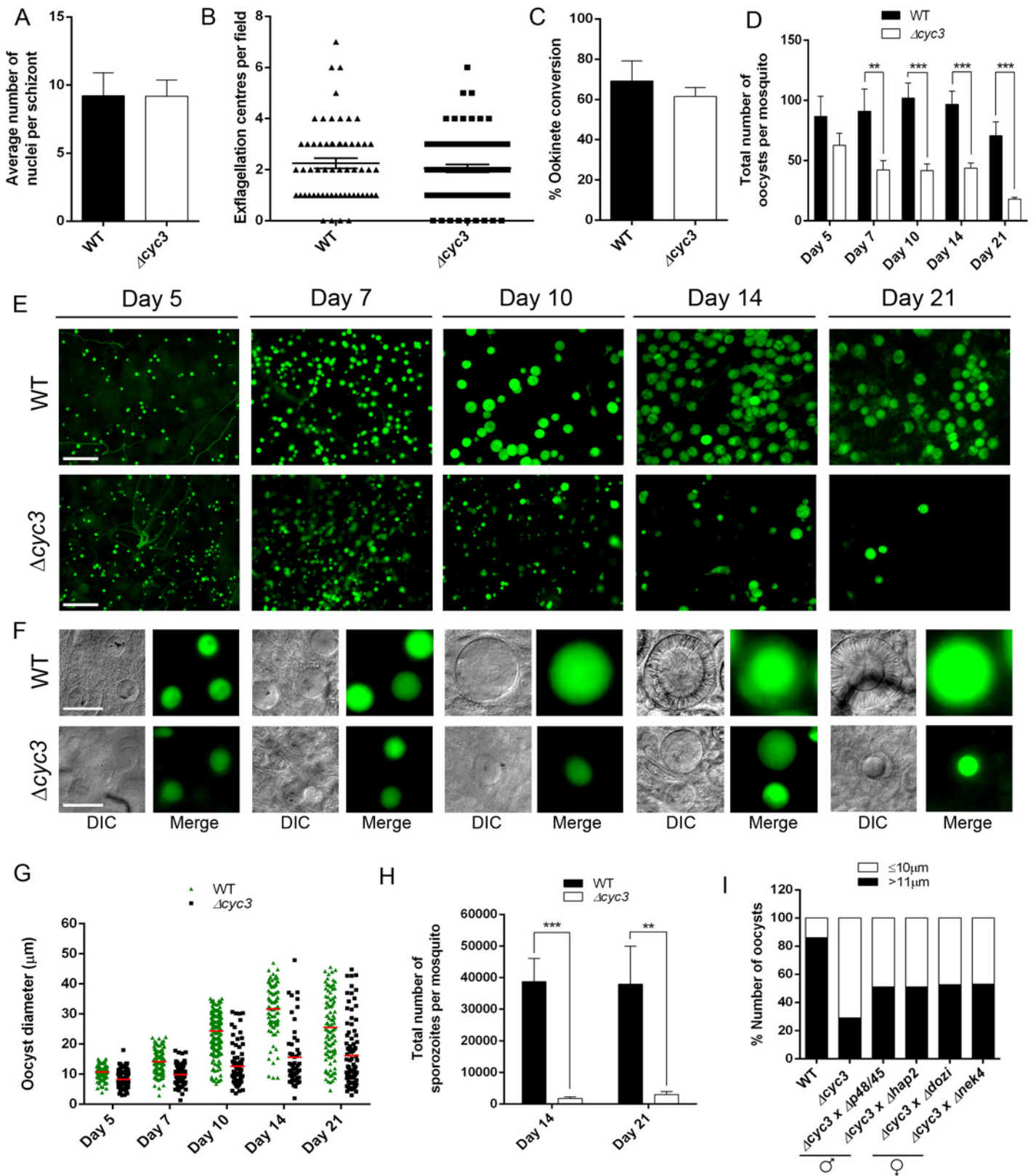




**Fig 3. CYC3 is dispensable in asexual and sexual stages but important for oocyst development.** (A) Average number of nuclei per schizont measured using Giemsa stained slides at 100x magnification. Bar is the mean  $\pm$  SEM.  $n = 4$  independent experiments. (B) Microgametogenesis of  $\Delta cyc3$  compared with WT measured as the number of exflagellation centres per field. Means  $\pm$  SEM are shown.  $n = 4$  independent experiments. (C) Ookinete conversion as a percentage in  $\Delta cyc3$  and WT lines. Ookinetes were identified using the marker 13.1 and defined as those cells that successfully differentiated into elongated 'banana shaped' ookinetes. Bar is the mean  $\pm$  SEM.  $n = 5$  independent experiments. (D) Total number of GFP-positive oocysts per infected mosquito, including normal and small oocysts, at 5, 7, 10, 14, 21 dpi for  $\Delta cyc3$  and WT lines. Bar is the mean  $\pm$  SEM.  $n = 3$  independent experiments (20 mosquitoes for each). Example of relative oocyst size and numbers at (E) 10x and (F) 63x magnification in  $\Delta cyc3$  and WT lines. Images show DIC and GFP at 5, 7, 10, 14 and 21 dpi. Scale bar = 100  $\mu m$  for 10x and 20  $\mu m$  for 63x. (G) Individual  $\Delta cyc3$  and WT oocyst diameters in  $\mu m$  at 5, 7, 10, 14 and 21 dpi. Horizontal line indicates the mean from 3 independent experiments (20 mosquitoes for each) of  $\Delta cyc3$  and WT.  $p < 0.001$  for all time points. (H) Total number of sporozoites per mosquito from 14 and 21 dpi midguts for  $\Delta cyc3$  and WT lines. Three independent experiments are described,  $n = 20$  mosquitoes for each replicate. \*\*  $p \leq 0.01$ , \*\*\*  $p \leq 0.001$ . (I) Genetic complementation of  $\Delta cyc3$ . Mosquitoes were fed with a combination of WT,  $\Delta cyc3$  or  $\Delta cyc3$  with either male ( $\Delta p48/45$  and  $\Delta hap2$ ) or female ( $\Delta dozi$  and  $\Delta nek4$ ) mutants. Shown is a representation of one experiment (20 mosquitoes per line).

doi:10.1371/journal.ppat.1005273.g003

however a significant reduction was observed at 7 dpi, which became even more evident at 10, 14 and 21 dpi (Fig 3D and 3E).

Furthermore, oocysts at 14 and 21 dpi appeared substantially smaller in  $\Delta cyc3$  compared with WT lines (Fig 3F). To quantify this reduction in oocyst size, the diameter of WT and  $\Delta cyc3$  oocysts was measured at multiple time points during development in three independent mosquito infections (Fig 3G). Even at early stages during oocyst development (5 and 7 dpi), we already detected a difference in mean oocyst diameter between  $\Delta cyc3$  and WT parasites (8  $\mu m$  and 11  $\mu m$  for 5 dpi; 10  $\mu m$  and 14  $\mu m$  for 7 dpi, respectively) and by 10 dpi, the majority of  $\Delta cyc3$  oocysts were substantially smaller than WT (12  $\mu m$  and 25  $\mu m$  mean diameter, respectively) (Fig 3F and 3G). This difference in oocyst size increased dramatically at 14 and 21 dpi as WT oocysts reached maturity (mean diameter of 31  $\mu m$  at 14 dpi compared to 15  $\mu m$  for  $\Delta cyc3$  oocysts, Fig 3G). The majority of  $\Delta cyc3$  oocysts were smaller in size even at 5 dpi. After this, although a small number of the  $\Delta cyc3$  oocysts continued to develop normally, the majority appeared to arrest and remained the same size until 21 dpi (Fig 3G).

In addition to the decrease in size, the number of  $\Delta cyc3$  sporozoites in infected mosquitoes was significantly reduced compared to WT in midguts at 14 and 21 dpi and in salivary glands at 21 dpi (Fig 3H, S4A and S4B Fig). However, when infected mosquitoes were allowed to feed on mice in bite-back experiments, we found that not only did transmission occur successfully but the pre-patent period for  $\Delta cyc3$  was the same as for WT parasites (S4A and S4B Fig). These data show that sporozoites produced from the few normal oocysts in the  $\Delta cyc3$  mutant are not affected in their efficacy of host infectivity.

Next we investigated whether the oocyst growth phenotype was related to a defect in ookinete structure, motility or DNA content. Ultrastructural analysis of ookinetes by transmission electron-microscopy revealed no morphological differences between  $\Delta cyc3$  and WT (S4C Fig). Similarly, both DNA content and the gliding motility of  $\Delta cyc3$  ookinetes were similar to WT (S4D and S4E Fig) suggesting that ookinetes are not affected by *cyc3* deletion.

Finally, we wanted to investigate whether *Plasmodium* CYC3 might function as a G1 or G2/M cyclin, which would explain the  $\Delta cyc3$  phenotype during sporogony. To this end, we examined the ability of a codon-optimized version of the *P. berghei cyc3* gene to complement a triple *cln* (G1 cyclin) mutant of the budding yeast *Saccharomyces cerevisiae* or a temperature sensitive growth phenotype of a *cdc13-117* B-type cyclin mutant of the fission yeast *Schizosaccharomyces pombe* (G2/M transition), respectively (S5A and S5B Fig). In both cases, *P. berghei cyc3* failed to rescue yeast cyclin mutant strains, suggesting that *P. berghei* CYC3 does not function as a classical G1 cyclin or G2/M cyclin under these conditions.

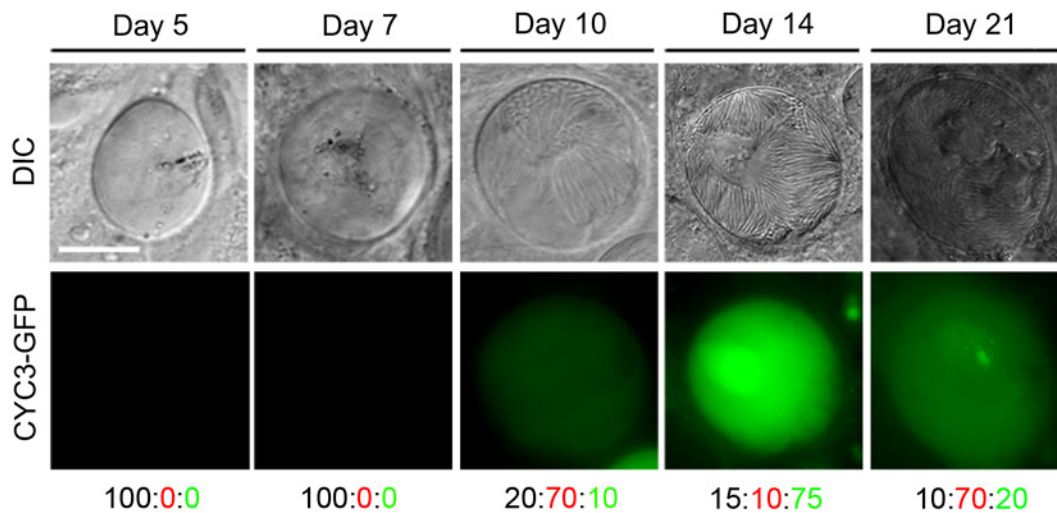


**Fig 4. Expression of CYC3-GFP during sporogony in mosquitoes.** Fluorescence microscopy of CYC3-GFP at different time points: 5, 7, 10, 14 and 21 dpi during development in the mosquito. Scale bar = 20  $\mu$ m. Representative percentage of oocysts that either: do not express GFP (black number), have a low expression of GFP (red number) or have a high expression of GFP (green number).

doi:10.1371/journal.ppat.1005273.g004

### CYC3 functions in both male and female lineages

Since CYC3-GFP was expressed in gametocytes (Fig 2B), we examined whether the defect in oocyst formation was sex-specific. To do this we performed genetic crosses between  $\Delta cyc3$  parasites and lines deficient in either male ( $\Delta p48/45$  and  $\Delta hap2$ ) or female ( $\Delta dozi$  and  $\Delta nek4$ ) gametes [45–48]. As scored by an increase in normal size oocysts at 14 dpi, we found that all mutants could only partially rescue the phenotype of the  $cyc3$  knockout, which affected both male and female lines equally (Fig 3I). These results reveal that the functional  $cyc3$  is inherited through both male and female lines and its function is independent of sexual commitment at the gametocyte stage (Fig 3I).

### CYC3-GFP expression shows a temporal pattern during sporogony

As the  $\Delta cyc3$  phenotype is observed during early oocyst development, we next examined CYC3-GFP expression during oocyst and sporozoite development at the same time points (5, 7, 10, 14 and 21 dpi) as described for the  $\Delta cyc3$  phenotypic analysis within mosquitoes using fluorescence microscopy (Fig 4).

Fluorescent imaging showed no detectable CYC3-GFP expression in oocysts at 5 and 7 dpi (representative images in Fig 4). Expression of CYC3-GFP was first observed at low levels in the majority of oocysts at 10 dpi with the highest expression detected at 14 dpi. Oocysts that had formed fully mature sporozoites showed the highest protein expression. After 14 dpi, we observed a decrease in CYC3-GFP expression in oocysts up to day 21pi (Fig 4).

### $\Delta cyc3$ parasites show defects in cell growth and sporozoite budding, with abnormal membrane fusion and vacuolation

To define further the defect in oocyst growth during different developmental stages of sporogony,  $\Delta cyc3$  and WT parasite-infected mosquito midguts at 7, 10, 14, and 21 dpi were examined by transmission electron microscopy. Marked differences were observed at the later time points in the ultrastructure of the majority of  $\Delta cyc3$  compared to WT oocysts, although some  $\Delta cyc3$  oocysts appeared similar to WT (Fig 5). At every time point there were significantly fewer

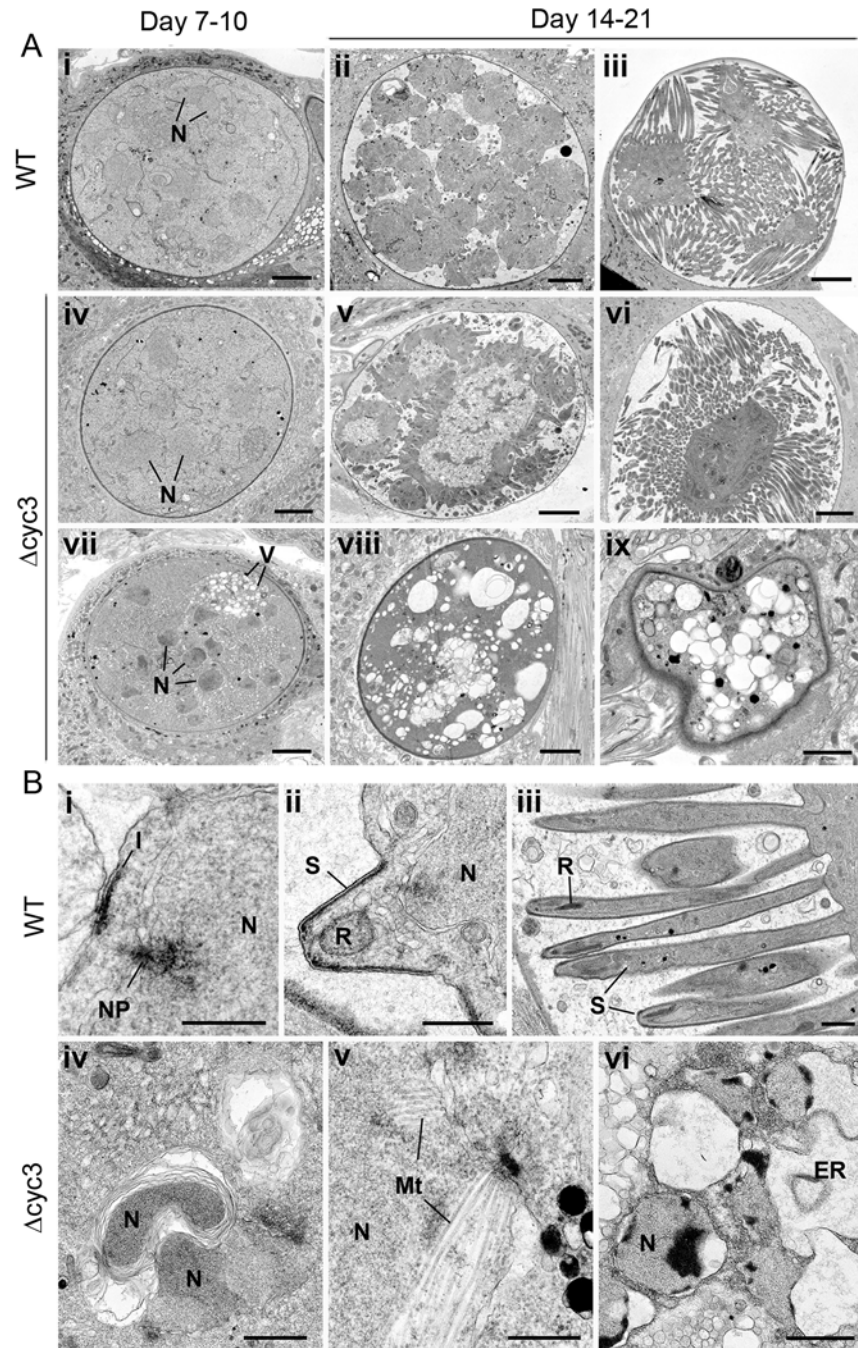


**Fig 5. Ultrastructure analysis of oocyst development in  $\Delta$ cyc3 mutant.** (A) Low power ultrastructural images of oocyst development at 7–10 days (i, iv, vii) and 14–21 days post-infection (dpi) showing normal sporulation of WT (ii, iii) and certain  $\Delta$ cyc3 (v, vi) parasites while other  $\Delta$ cyc3 mutants show evidence of cytoplasmic vacuolation (V) and degeneration (vii, viii, ix). N—nucleus. Bars represent 10  $\mu$ m. (B) Details showing progressive stages in sporozoite formation in wild type parasites (i–iii) and various abnormal developmental stages of the  $\Delta$ cyc3 parasite (iv–vi). Bars represent 1  $\mu$ m. i. Initiation of sporozoite formation with formation of the inner membrane complex (I) beneath the plasmalemma and above a peripherally located nucleus (N) with nuclear pole (NP). ii. Early sporozoite (S) with rhoptry Anlagen (R) budding from the surface of the sporoblast. N—nucleus. iii. Late stage in sporozoite formation showing the elongated sporozoites (S). R—rhoptry. iv. Detail of the sporoblast cytoplasm showing nuclei (N) enclosed by abnormal membrane whorls v. Part of a nucleus with extensive nuclear spindle microtubule (Mt) not seen in WT parasite. vi. Detail of a late stage in parasite degeneration showing apoptotic-like nuclei (N) and dilated endoplasmic reticulum (ER).

doi:10.1371/journal.ppat.1005273.g005

oocysts in the guts of mosquitoes infected with  $\Delta cyc3$  compared to the WT parasites (5 oocysts/gut  $\Delta cyc3$  compared to 60 oocyst/gut WT at 7 dpi).

At 7 and 10 dpi the oocysts of both the WT and  $\Delta cyc3$  had similar structural appearance being spherical with the cytoplasm completely filling the cyst (Fig 5Ai, 5Aiv and 5Avii). The cytoplasm contains numerous nuclear profiles and homogenous appearing cytoplasm containing mitochondria and apicoplasts. However, a proportion (approximately 10%) of the  $\Delta cyc3$  oocysts also showed centrally located nuclei and exhibited some vacuolation of the cytoplasm (Fig 5Avii). By 14 dpi, the majority (>98%) of WT oocysts exhibited various stages of sporozoite formation (Fig 5Aii, 5Aiii and 5Bi–5Biii) or oocysts with mature sporozoites (Fig 5Aiii). In contrast, there were many fewer  $\Delta cyc3$  oocysts (10  $\Delta cyc3$  compared to 60 WT oocysts) and only a proportion (<40%) of these showed similar features of sporulation (Fig 5Av and 5Avi). Many (>60%) of the  $\Delta cyc3$  oocysts showed no evidence of sporulation (Fig 5Aviii and 5Aix). These oocysts showed no retraction of the plasmalemma to form the sporoblasts and there was no evidence of the initiation of sporozoite formation (Fig 5Aviii and 5Aix). However, cytoplasmic changes were observed including abnormal membrane reduplication (Fig 5Biv) and nuclei containing large numbers of microtubules, suggesting mitosis and cytokinesis were affected (Fig 5Bv). There was evidence of nuclei with apoptotic-like chromatin changes and dilated endoplasmic reticulum (Fig 5Bvi). There appeared to be continued cytoplasmic vacuolation consistent with progressive cell death (Fig 5Aviii, 5Aix and 5Bvi). These results are consistent with the idea that DNA synthesis, endomitosis and cytokinesis are severely defective in most but not all oocysts. Moreover, structural abnormalities in some  $\Delta cyc3$  oocysts suggest that they are incapable of forming viable sporozoites.

### Transcriptome analysis of $\Delta cyc3$ parasites reveals modulated expression of genes involved in signalling, ookinete invasion, and oocyst development

The marked changes in  $\Delta cyc3$  oocyst morphology and growth led us to analyse the regulation of mRNA in  $\Delta cyc3$  parasites compared with WT. We first used strand-specific RNA sequencing (RNA-seq) to investigate the global transcript levels in  $\Delta cyc3$  and WT activated gametocytes and ookinetes. The deletion of *cyc3* was confirmed by RNAseq, with no reads mapping to the region of the gene targeted for disruption (S6A Fig). Generally, most transcript levels were very similar in activated gametocytes, with strong linkage between levels in  $\Delta cyc3$  and WT lines. However, the ookinete transcriptome was greatly altered by loss of *cyc3*, with many genes down-regulated and a smaller number up-regulated. In total, 813 and 2,069 genes showed modulated expression in activated gametocytes and ookinetes, respectively ( $p < 0.05$  and fold change  $> 2$ ; 702 and 1,891 genes in activated gametocytes and ookinetes, respectively, with  $p < 0.01$  and fold change  $> 2$ ) (Fig 6A, S6B Fig and S2 Table), including those with roles in reversible phosphorylation, transcription, cell signalling and inner membrane complex function (Fig 6B, S6C Fig and S3 Table). We identified several functional clusters that were significantly differentially expressed in  $\Delta cyc3$  (Fig 6B, S6C Fig and S3 Table) which may be collectively responsible for the observed phenotype. Global Gene Ontology (GO) analysis showed enrichment of genes associated with GO terms ‘kinase activity’, ‘protein phosphorylation’ and ‘inner membrane complex’ (S6D Fig).

To validate our RNA-seq data, we performed qRT-PCR analysis of specific sets of genes known to have roles in cell cycle, signalling and transcription, or invasion and oocyst development (Fig 6C and S2 Table). These data showed very good correlation with the RNA-seq results (Fig 6D) validating the results for activated gametocytes and ookinetes. In addition, qRT-PCR data were collected for schizonts and/or day 14 oocysts (Fig 6C); these data showed that most

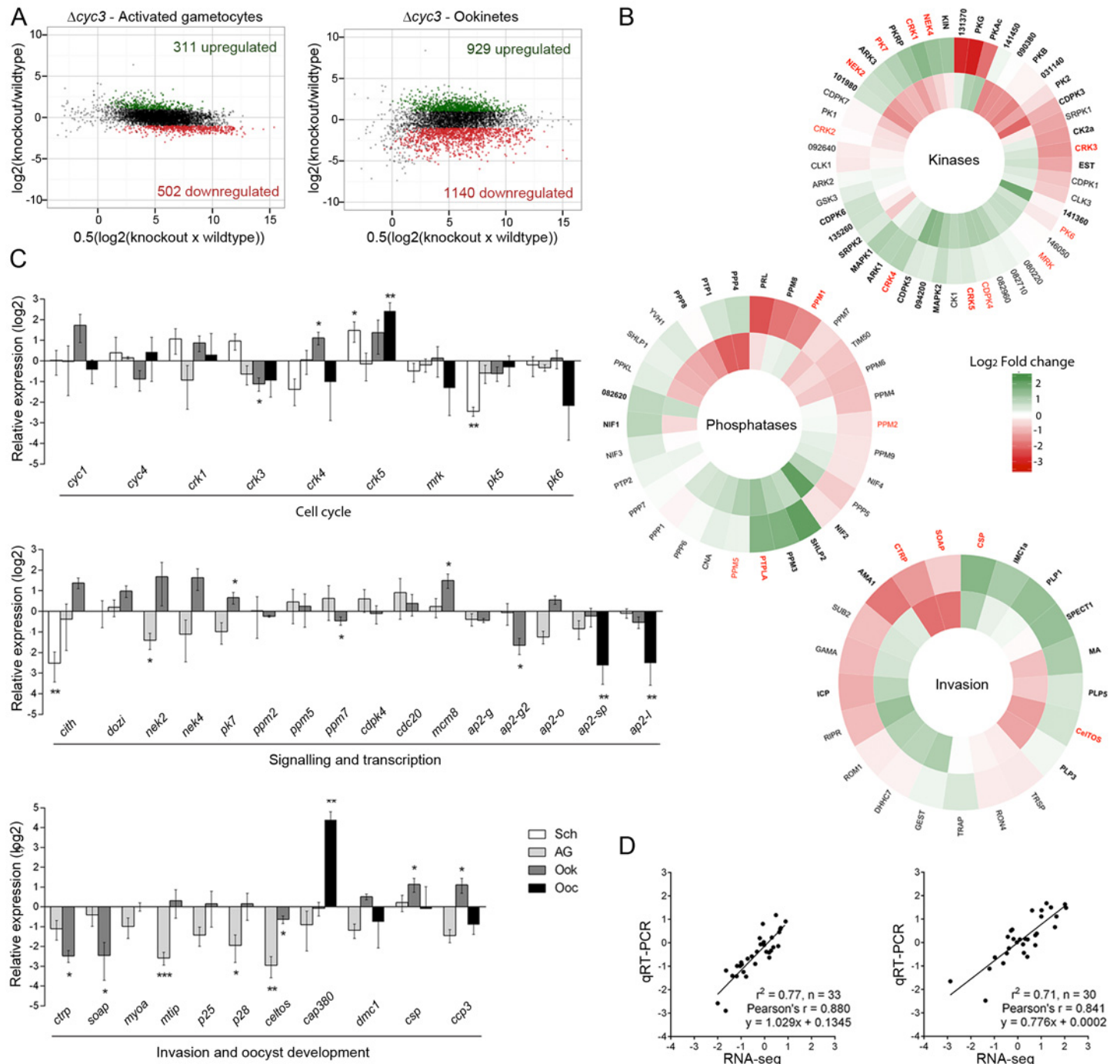


**Fig 6. Transcript analysis of genes involved in parasite development.** (A) Ratio-Intensity scatter plots for  $\Delta cyc3$  activated gametocytes and ookinetes. The y-axis shows the log<sub>2</sub> fold change between wild-type and mutant and the x-axis shows the average of normalised FPKM (See also S2 Table). Significantly up-regulated genes are highlighted in green while down-regulated genes are highlighted in red. (B) Heatmaps for invasion, kinase and phosphatase gene clusters based on their log<sub>2</sub> fold change in  $\Delta cyc3$  activated gametocytes (inner track) and  $\Delta cyc3$  ookinetes (outer track) relative to WT. Functional groups were inferred from annotations available in GeneDB (<http://www.genedb.org>). Genes that were found significantly misregulated are shown in bold and those validated by qRT-PCR are shown in red. Full gene list and functional clusters are shown in S3 Table. (C) Log<sub>2</sub> fold transcript change in  $\Delta cyc3$  at different life-cycle stages of cell cycle, signalling and transcription genes, and invasion and oocyst development genes, studied in  $\Delta cyc3$  (compared against WT) using qRT-PCR. Data were normalised against an endogenous control gene, *hsp70* (PBANKA\_081890). Each bar is the mean of relative expression in comparison to WT from three biological replicates  $\pm$  SEM. Sch: schizonts; AG: activated gametocytes; Ook: ookinetes; Spor: 14 dpi oocysts/sporozoitcs. \*  $p < 0.05$ ; \*\*  $p < 0.01$ , \*\*\*  $p < 0.001$ . (D) Comparison of qRT-PCR and RNA-seq data (Cuffdiff2 analysis) using Log<sub>2</sub> values for activated gametocyte and ookinete samples.

doi:10.1371/journal.ppat.1005273.g006

of the changes in transcript levels for these sets occur at the ookinete stage, with some additional effects in oocysts.

Importantly, both RNA-seq and qRT-PCR analyses showed that neither of the other two *Plasmodium* cyclin genes were differentially expressed in response to deletion of *cyc3*, suggesting that there is no compensation provided by up-regulation of other cyclins. In contrast, several of the *cdks* were differentially expressed at different stages (Fig 6C): of particular interest was *crk1* and *crk5*, which were significantly up-regulated in ookinetes and are known to have roles in gene transcription [49] and cell cycle [50], respectively.

Recently, it has been shown that a family of transcription factors (apiAP2) is responsible for gametocyte commitment, as well as ookinete and sporozoite development [36,51–55]. This family is also a feature of chromerid genomes and their evolutionary history suggests they have mediated evolutionary changes during lineage differentiation [56]. Our analysis showed that several apiAP2 family members were affected by *cyc3* deletion, notably a significant down-regulation of *ap2-sp* and *ap2-l* in  $\Delta$ *cyc3* ookinetes and oocysts, consistent with a reduction in normal oocyst formation (Fig 6C, S6C Fig and S2 Table). Due to the important role of reversible phosphorylation in cell cycle progression in other systems [3], we next looked at the expression of protein kinases, phosphatases and cell cycle proteins involved in parasite development, especially those that either display a similar phenotype to that of  $\Delta$ *cyc3* when deleted (*pk7*, *ppm5*) or are involved in sexual development (*nek4*). The expression of genes involved in male sexual development (*cdpk4* and *cdc20*) [29,57,58] was not significantly affected. Furthermore, the transcription of *ppm7*, *ppm5* and *pk7*, which have similar protein localisation and/or similar phenotypes in gene knock-out lines [30,31], were also unaffected (Fig 6C). However, two genes important for zygote differentiation (*nek2* and *nek4*) [47,59] were significantly mis-regulated in activated gametocytes and ookinetes. Based on the phenotype observed in  $\Delta$ *cyc3* parasites and the fact that several known invasion genes were significantly affected, as detected in the RNA-seq analysis, we next focused on genes involved in ookinete invasion and oocyst development. Interestingly, there was a marked down-regulation of genes required for ookinete motility and invasion (Fig 6C), such as *mtip*, *ctrp* and *soap* [60,61], despite the fact that ookinete development and motility appeared to be unaffected (S4 Fig). Genes known to be required during oocyst development, such as *cap380*, coding for a capsule protein necessary for healthy oocyst formation and subsequent transmission [62], and *csp*, important for infectivity of the host [63], were mis-regulated in multiple stages (Fig 6C). These data suggest that the oocyst development phenotype in  $\Delta$ *cyc3* may be a downstream consequence of the mis-regulation of these genes, well before sporogony commences.

Overall, deletion of *cyc3* caused the modulated expression of a number of genes related to the observed phenotype, especially in ookinetes, including transcription factors, putative cyclin binding partners, and genes for signalling and subsequent oocyst development.

## Discussion

The molecular mechanisms controlling the cell cycle and mitosis are regulated by key molecules including CDKs and cyclins. Cyclins are key regulators of CDKs and are synthesised and degraded at specific phases of the cell cycle [5,64]. Although cdk/cyclins have been well studied in many eukaryotic model systems, their role in the unicellular parasite *Plasmodium* is not well understood. Here, we show that despite its complex and atypical pattern of cell cycle and division, *Plasmodium* only has three cyclin genes, a very small complement compared to other organisms including human (30 annotated genes in the Refseq dataset), yeast (22 genes) and *Drosophila* (12 genes). *Plasmodium* has no Group I cyclins but has homologues belonging to Group II (CYC3) and Group III (CYC1 and CYC4). CYC3 is a P-type cyclin, a family which

contains many cyclins of plants (CYCPs) [17]. It also shows similarity to PHO80 cyclin from *Saccharomyces cerevisiae* [20] and a G1 cyclin present in kinetoplastids [65,66]. Both Pho80 and plant CYCPs appear to link cell cycle regulation to nutritional status: in yeast, Pho80 and other P-like cyclins associate with CDK Pho85 to phosphorylate a variety of substrates involved in phosphate, glycogen and carbon source metabolism (reviewed in [16]), whereas CYCP2;1 in *Arabidopsis* is required for G2/M transition in meristem activation in a nutrition-responsive manner [18]. Trypanosomes encode at least three P-type cyclins, CYC2, 4, and 7, with CYC10 and 11 being likely divergent members of the family (“Pho80-like” cyclin *TbCYC5* [66] is a cyclin Y, see S1 Fig). In contrast to CYCP, *Trypanosoma brucei* CYC2 is required for progression from G1 phase in the insect stage of the parasite [67], which would put its cell cycle activity in a position more akin to the Pho80-like cyclins (Pcls) in yeast [16]. In keeping with this, *TbCYC2* is able to rescue a yeast CLN mutant [19], in which 3 Group I G1 cyclins, *CLN1*, 2 and 3, were inactivated [68].

There are only three clearly identifiable CDKs (*PfPK5*, *Pfcrk1* and *Pfcrk3*) in the *Plasmodium* genome [31,69]. The lack of cyclin D in *Plasmodium* here mirrors the absence of CDK4/6 orthologues previously reported [49], and *Pfcrk1* is a CDK10/11-related protein [69], which matches well with the presence of cyclin L family members identified here. Moreover, a fourth protein, *Pfmrk*, was initially described as a CDK7 homologue and was shown to be stimulated by binding to human cyclin H *in vitro* [70], but subsequent work showed that its affinities are less clear [69] and functional work suggests it might be a RNA polymerase II carboxyl-terminal domain kinase rather than a CDK [71]. There is no homologue of Pho85 identified in *Plasmodium* and the essential kinase *PfPK5* is a relative of CDK1/2, which would normally be activated by a Group I cyclin in animals or fungi.

Transcription of *P. berghei* cyclins varies during different phases of the life cycle with the highest transcription seen in gametocytes and schizonts [35]. Our localisation studies of CYC3-GFP by fluorescence and deconvolution microscopy showed both cytoplasmic and nuclear localisation, which is expected given the localisation and role of most cyclins in model systems [10]. The subcellular location of P-type cyclins (for example, CYCP2;1) in plants is mainly nuclear [18], however, *TbCYC2* is also expressed in the cytosol of procyclic forms and controls posterior morphogenesis of the parasite during the G1/S and G2/M transition [19,65,66,72].

A recent study on the AP2-O transcription factor in *Plasmodium* showed that *cyc3* is a target of AP2-O and used deletion of *cyc3* as a validation tool to show that it had a role in ookinete to oocyst development [36]. Our gene deletion mutant is consistent with this analysis in terms of number and size of oocysts, but further dissects in depth the function of *cyc3* throughout the lifecycle using transcriptome analysis and high resolution microscopy. Maturation of most of the  $\Delta$ *cyc3* oocysts, based on their abnormal shape and size, was impaired in infected mosquito guts, and detailed studies revealed that this defect in oocyst growth and differentiation began during early sporogony. *Plasmodium* oocysts contain a highly lobed syncytial nucleus that divides at the time of sporozoite budding into a number of lobes, which undergo subsequent mitotic division resembling endomitosis [23,25]. The  $\Delta$ *cyc3* phenotype suggests that although initial oocyst formation occurs, in many of the oocysts the division of nuclear lobes with oocyst growth is drastically affected and further budding of sporozoites from these lobes does not occur. This defect leads to abnormalities in membrane formation, vacuolation and subsequent cell death during the later stages of sporogony. The characteristics of  $\Delta$ *cyc3* oocyst development suggest that maturation and differentiation are arrested, with cells unable to progress further to form additional lobes and start sporozoite budding and mitotic division.

A number of gene deletion mutants have been described in *Plasmodium* that affect oocyst maturation for example; *PbCAP380*, affecting oocyst capsule formation [62]; *PbGEX* and

*PbDMC1*, affecting oocyst size and sporozoite formation [73,74]; *PbLAPs* and *PbCDLK*, affecting sporogony but not the size of the oocyst [31,75,76]; *PbMISFIT*, causing small sized oocysts [77]; and G actin sequestering protein (C-CAP) affecting oocyst development and showing similar features to  $\Delta cyc3$  during early oocyst development [78]. However, the phenotype of  $\Delta cyc3$  lines differs from that of all these mutants due to the fact that some normal oocysts are produced, which are able to form invasive salivary gland sporozoites and initiate liver stage infection. Moreover, none of the other mutated genes was implicated in cell cycle control or cell division. The presence of a small number of normal oocysts/sporozoites in the  $\Delta cyc3$  mutant does suggest that CYC3 has a subtle role in oocyst/sporozoite development. The reduction in sporozoite number (in addition to the reduction in oocyst number) is drastic at 14 and 21 dpi compared to the WT parasites and there is clear expression of CYC3-GFP in 14 dpi oocysts, both indicative of a role in sporozoite development. This might suggest that there are unknown regulatory mechanisms involved in the control of the oocyst development that can by-pass a default CYC3-dependent pathway to some degree in these parasites during early oocyst development and sporogony.

Specific protein kinase and phosphatase mutants (*PbPK7* and *PbPPM5*) show some resemblance to the  $\Delta cyc3$  phenotype, with a reduced number of oocysts, which were abnormally small and did not complete sporogony before arresting [30,31]. However, only minor changes in the transcript level of protein kinase (*pk7*) or phosphatase (*ppm5*) were detected. Conversely, *cyc3* transcripts are down-regulated in  $\Delta ppm5$  parasites [30] suggesting that PPM5 acts upstream of CYC3.

Gene deletion revealed that CYC3 is dispensable during asexual multiplication in erythrocytes and in the liver (erythrocytic and exo-erythrocytic schizogony) and sexual development during male gametogenesis. However, CYC3 clearly modulates sporogony via endomitotic multiplication during oocyst development in the mosquito. Oocysts are the only replicative extracellular stage during the parasite life cycle, and therefore it is possible that CYC3 modulates this extracellular replication in response to metabolic sensing within the mosquito. For example, *Arabidopsis* CYCP2;1 is transcribed in response to sugar signals by a specific transcriptional factor, allowing cell cycle progression [18]. CYC3 may have a direct or indirect role in regulation of transcription in the ookinete, of specific genes involved in oocyst growth (defined as a G1 phase) and sporogony (defined as S/mitotic phases), and that could explain why we see expression of CYC3-GFP in ookinetes and 10 to 14 dpi oocysts. Rescue experiments in yeast suggest that *Plasmodium* CYC3 does not behave as a classical G1 or G2/M cyclin, or at least cannot substitute for the function of yeast cyclins. Nevertheless the peak in expression of CYC3-GFP around 10 to 14 dpi of oocyst development, just before sporogony, and the defect in sporozoite production in  $\Delta cyc3$  mutants, are both consistent with a cyclin-B-like role in cell cycle progression and a role in G1/S progression.

Global transcript analysis of the  $\Delta cyc3$  mutant suggested that neither *cyc1* nor *cyc4* compensates for the *cyc3* deletion. Analysis of all the CDKs showed that several, including *crk1*, with a role in transcription [49], were mis-regulated at several stages in  $\Delta cyc3$  parasites; however it is unlikely that transcription of a putative CDK partner would be controlled by CYC3. It has been reported previously that *PfCYC3* binds and activates the CDK1 homologue, *PfPK5*, *in vitro* [35], and a similar result was reported for the homologues from *Eimeria tenella* [79], although we saw no significant mis-regulation of *pk5* in  $\Delta cyc3$  parasites and no study has shown a *Plasmodium* cyclin-CDK interaction *in vivo*. Other cell cycle genes were affected including predicted members of the mini chromosome maintenance (MCM) family. While no MCM has been functionally characterised in *Plasmodium*, the MCM family has been bioinformatically well classified in *Apicomplexa* [80,81] and MCMs are known to be important for G1/S phase progression and initiation of DNA replication [82].



Misregulation of genes involved in ookinete invasion and structure (such as *mtip*, *ctrp* and *soap*) had no observable effect on ookinete motility or oocyst formation at 5 dpi and we observed no detectable phenotype with electron microscopy, however, a subtle delay in oocyst initiation (due to ookinete invasion or motility) may be enough to initiate deleterious consequences downstream during oocyst development. In addition to this, we cannot rule out the possibility that CYC3 is indirectly involved in nutrient/environmental sensing in the mosquito gut, a known function of cyclins in other systems [18]. The mis-regulation of these, as yet undefined, genes may be responsible for the mixed population of small, defective oocysts versus normal, healthy oocysts. Thus, the absence of *cyc3* may make these parasites more sensitive to environmental stimuli such as nutrient abundance, or the impact of developmental mis-timing (via mis-regulation of invasion genes).

Oocyst growth may further deteriorate following the mis-regulation of genes required for oocyst development (such as *cap380*). Transcription analysis also showed that several members of the apiAP2 transcription factor family, which have been shown to regulate various stages of development, were affected in  $\Delta cyc3$  oocysts. This is perhaps unsurprising considering that normal regulation of these genes is required for successful oocyst development [52,53,55]. Global transcriptomics is a useful tool for the identification of possible dysregulation and compensatory mechanisms in  $\Delta cyc3$  parasites however the measurement of mRNA levels is not necessarily indicative of the corresponding protein levels. Future proteomic work may provide more information on protein-protein interactions between CYC3 and putative CDK partners or on the effects of *cyc3* deletion on global (or cell cycle specific) protein levels in the  $\Delta cyc3$  mutant.

In conclusion, this is the first study to classify phylogenetically the cyclins in *Plasmodium* and uncover, in depth, an important function for CYC3, a novel P-type cyclin. We describe a key role for this cyclin during the early stages of ookinete to oocyst development, specifically the G1/S phase, which subsequently affects differentiation and sporogony, suggesting it is a modulator of transcription and oocyst endomitotic development in *Plasmodium*.

## Materials and Methods

### Ethics statement

All animal work at Nottingham has passed an ethical review process and was approved by the United Kingdom Home Office. Work was carried out in accordance with the United Kingdom 'Animals (Scientific Procedures) Act 1986' and in compliance with 'European Directive 86/609/EEC' for the protection of animals used for experimental purposes under UK Home Office Project Licenses 40/3344 and 30/3248. Sodium pentobarbitol was used for terminal anaesthesia and a combination of ketamine followed by antisedan was used for general anaesthesia. All efforts were made to minimise animal suffering.

### Animals

Six-to-eight week old female Tuck-Ordinary (TO) (Harlan) outbred mice were used for all experiments.

### Bioinformatic analysis of cyclins

To identify cyclin-like proteins, a pan-cyclin hidden Markov model was used to perform a similarity search using HMMER3 [83]. Briefly, all annotated cyclins were taken from the predicted proteomes of human, *Arabidopsis thaliana*, *Caenorhabditis elegans*, *Saccharomyces cerevisiae*, *Schizosaccharomyces pombe*, and *Toxoplasma gondii*. These cyclins were aligned using

MAFFTv6.925b [84] with the L-INS-i strategy [85], trimmed to conserved regions and used to create a HMM, which was used to search the predicted proteomes of 12 apicomplexan parasites (EuPathDB; <http://eupathdb.org>; see Fig 1C) as well as 20 other eukaryotes from diverse groups. The conserved cyclin domains were excised from these sequences based on HMM hits with e-values  $\leq 10^{-18}$ , realigned and used to create a refined HMM, which was then used to re-search the apicomplexan proteomes at a threshold of e-value  $\leq 10^{-12}$ . Alignments of cyclins were trimmed to conserved regions and used to infer maximum likelihood phylogenies as implemented by the program PhyML3.0 [86] using the LG substitution matrix with a gamma-distributed variation in substitution rate approximated to 4 discrete categories (shape parameter estimated from the data). Trees shown are a majority-rule consensus of 100 bootstrap replicates for each alignment.

## Generation of transgenic parasites

For GFP-tagging by single homologous recombination [30], a 986 bp region of *cyc3* starting 332 bp upstream of the ATG start codon and omitting the stop codon was amplified using primers T0891 and T0892. This was inserted upstream of the *gfp* sequence in the p277 vector using KpnI and ApaI restriction sites. The p277 vector contains the human *dhfr* cassette, conveying resistance to pyrimethamine. Before transfection, the sequence was linearised using HindIII,

The gene targeting vector for  $\Delta cyc3$  lines was constructed using the pBS-DHFR plasmid, which contains polylinker sites flanking a *T. gondii dhfr/ts* expression cassette conveying resistance to pyrimethamine, as described previously [31]. PCR primers N0451 and N0452 were used to generate a 411 bp fragment of 5' upstream sequence of *cyc3* from genomic DNA, which was inserted into ApaI and HindIII restriction sites upstream of the *dhfr/ts* cassette of pBS-DHFR. A 663 bp fragment generated with primers N0453 and N0454 from the 3' flanking region of *cyc3* was then inserted downstream of the *dhfr/ts* cassette using EcoRI and XbaI restriction sites. The linear targeting sequence was released using ApaI/XbaI. All of the oligonucleotides used to make these constructs can be found in S1 Table.

*P. berghei* ANKA line 2.34 (for GFP-tagging) or ANKA line 507c11 (for gene deletion [44]) were then transfected by electroporation [44]. Briefly, electroporated parasites were mixed immediately with 100  $\mu$ l of reticulocyte-rich blood from a phenylhydrazine (6mg/ml, Sigma) treated, naïve mouse, incubated at 37°C for 20 min and then injected intraperitoneally. From day 1 post infection pyrimethamine (70  $\mu$ g/ml, Sigma) was supplied in the drinking water for four days. Mice were monitored for 15 days and drug selection was repeated after passage to a second mouse. Resistant parasites were then used for cloning by limiting dilution and subsequent genotyping.

## Genotypic analysis of mutants

For the C-terminal fusion GFP-tagged parasites, a diagnostic PCR reaction was used as illustrated in S2 Fig. Primer 1 (INT T89) and Primer 2 (ol492) were used to determine correct integration of the *gfp* sequence at the targeted locus (S1 Table). After confirmation of correct integration, genomic DNA from wild type and transgenic parasites was digested with BsmI and the fragments were separated on a 0.8% agarose gel, blotted onto a nylon membrane, and probed with a PCR fragment homologous to the *P. berghei* genomic *cyc3* sequence cloned in the p277 vector, using the Amersham ECL Direct Nucleic Acid Labelling and Detection kit (GE Healthcare). Parasites were also visualised on a Zeiss AxioImager M2 (Carl Zeiss, Inc) microscope fitted with an AxioCam ICc1 digital camera (Carl Zeiss, Inc) and analysed by Western blot to confirm GFP expression and the correct protein size.

For the gene knockout parasites, two diagnostic PCR reactions were used as shown in [S3 Fig](#). Primer 1 (INT N45) and primer 2 (ol248) were used to determine successful integration of the selectable marker at the targeted locus. Primers 3 (N45 KO1) and 4 (N45 KO2) were used to verify deletion of the gene. After confirmation of integration, genomic DNA from wild type and mutant parasites was digested with HindIII and the fragments were separated on a 0.8% agarose gel, blotted onto a nylon membrane (GE Healthcare), and probed with a PCR fragment made with primers N0453 and N0454 which is homologous to the *P. berghei* genomic DNA just outside of the targeted region. All of the oligonucleotides used to genetically confirm these mutant parasite lines can be found in [S1 Table](#).

Chromosomes of wild type, gene knockout and GFP-tagged parasites were separated by pulsed field gel electrophoresis (PFGE) on a CHEF DR III (BioRad) using a linear ramp of 60–500 s for 72 h at 4 V/cm. Gels were blotted and hybridized with a probe recognizing both the resistance cassette in the targeting vector and, more weakly, the 3'UTR of the *P. berghei dhfr/ts* locus on chromosome 7.

## Phenotypic analysis

To record the nuclei number per schizont, merozoites in late schizonts were counted 18–24 hours after schizont cultures were made. Exflagellation was examined on day 4 to 5 post-infection. Ten  $\mu$ l of gametocyte-infected blood was obtained from the tail with a heparinised pipette tip and mixed immediately with 40  $\mu$ l of ookinete culture medium (RPMI1640 containing 25 mM HEPES, 20% fetal bovine serum, 10 mM sodium bicarbonate, 50  $\mu$ M xanthurenic acid at pH 7.6). The mixture was placed under a Vaseline-coated cover slip and 15 min later exflagellation centres were counted by phase contrast microscopy in 12–15 fields of view using a 40 $\times$  objective and 10 $\times$  ocular lens. Ookinete formation was assessed the next day. Ten  $\mu$ l of infected tail blood was obtained as above, mixed immediately with 40  $\mu$ l ookinete culture medium, and incubated for 2 hours at 20°C to allow completion of gametogenesis and fertilisation. Each culture was then diluted with 0.45 ml of ookinete medium and incubated at 20°C for a further 21–24 hours to allow ookinete differentiation. Cultures were pelleted for 2 min at 5000 rpm and then incubated with 50  $\mu$ l of ookinete medium containing Hoechst 33342 DNA dye to a final concentration of 5  $\mu$ g/ml and a Cy3-conjugated mouse monoclonal antibody 13.1 [58] recognizing the P28 protein on the surface of ookinetes and any undifferentiated macrogametes or zygotes. P28-positive cells were counted with a Zeiss AxioImager M2 microscope (Carl Zeiss, Inc) fitted with an AxioCam ICc1 digital camera. Ookinete conversion was expressed as the percentage of P28 positive parasites that had differentiated into ookinetes [45].

For mosquito transmission experiments 20–50 *Anopheles stephensi* SD500 female mosquitoes were allowed to feed for 20 min on anaesthetised infected mice whose asexual parasitaemia had reached ~12–15% and were carrying comparable numbers of gametocytes as determined by Giemsa stained blood films. Days 5, 7, 10, 14, and 21 days post-infection (dpi) 20 mosquitoes were dissected and oocysts on their midguts counted. Oocyst formation was examined following Hoechst 33342 staining in PBS for 10–15 min and guts were mounted under Vaseline-rimmed cover slips. Counting and images were recorded using 10 $\times$  and 63 $\times$  oil immersion objectives on a Zeiss AxioImager M2 microscope fitted with an AxioCam ICc1 digital camera. At 14 and 21 dpi, the same mosquito midguts used to record the oocyst number were homogenised in a loosely fitting homogeniser to release sporozoites, which were then quantified using a haemocytometer. Only for 21 dpi mosquitoes, salivary glands were dissected and homogenised in a loosely fitting homogeniser to release sporozoites, which were then quantified using a haemocytometer. Due to day-to-day variations in transmission levels, all data were normalised to a matching number of wild type controls analysed on the same day. Mosquitoes infected

with wild type or  $\Delta cyc3$  parasites were used to perform bite back experiments with a TO mouse each in three independent experiments. Blood stage parasitaemia was measured for wild-type and  $\Delta cyc3$  by Giemsa staining at 4 dpi.

Oocyst diameter was measured with the AxioVision Imager software from images of 50–60 oocysts, in triplicate for 5, 7, 10, 14 and 21 dpi using a 63x oil immersion objective on a Zeiss AxioImager M2 microscope fitted with an AxioCam ICc1 digital camera.

For genetic complementation, we used either male ( $\Delta p48/45$  and  $\Delta hap2$ ) or female ( $\Delta dozi$  and  $\Delta nek4$ ) parasites using a method described previously [30]. Briefly, mice were infected with combinations of the different parasite lines mentioned above and subsequently fed to 3–6 day old mosquitoes. These were dissected 12–14 dpi and the diameter of oocysts was determined as mentioned above. Statistical analyses were performed using GraphPad Prism (GraphPad Software). For comparison between  $\Delta cyc3$  and WT, an unpaired Student's *t*-test was used.

For the fluorescence pictures of CYC3-GFP oocysts, mosquito midguts have been dissected at 5, 7, 10, 14 and 21 dpi and images were recorded using 63x oil immersion objectives on a Zeiss AxioImager M2 microscope fitted with an AxioCam ICc1 digital camera.

## Western blotting

Schizont, gametocyte and ookinete samples were isolated as described below. WT-GFP or CYC3-GFP samples were then purified using a GFP-Trap kit to immunoprecipitate GFP-fusion protein (Chromotek). After the addition of Laemmli sample buffer, the samples were boiled and an equal concentration of total protein was loaded on a 4–12% SDS-polyacrylamide gel. Samples were subsequently transferred to nitrocellulose membranes (Amersham Biosciences) and immunoblotting performed using the Western Breeze Chemiluminescent Anti-Rabbit kit (Invitrogen) and anti-GFP polyclonal antibody (Invitrogen) at a concentration of 1:1250, according to the manufacturer's instructions.

## Electron microscopy

Ookinete samples (described below) and mosquito midguts at 7, 10, 14 and 21 dpi were fixed in 4% glutaraldehyde in 0.1 M phosphate buffer and processed for routine electron microscopy as previously described [87]. Briefly, samples were post fixed in osmium tetroxide, treated *en bloc* with uranyl acetate, dehydrated and embedded in Spurr's epoxy resin. Thin sections were stained with uranyl acetate and lead citrate prior to examination in a JEOL1200EX electron microscope (Jeol UK Ltd).

## Purification of schizonts, gametocytes, ookinetes and oocysts

Purification of gametocytes was achieved using a protocol modified from [88]. Mice were treated by intra-peritoneal injection of 0.1 ml of phenylhydrazine (6 mg/ml, Sigma) in PBS to encourage reticulocyte formation four days prior to infection with parasites. Four days after parasites injection in mice, mice were treated with sulfadiazine (Sigma) at 20 mg/L in their drinking water for two days to eliminate asexual blood stage parasites. On day six post-injection (p.i), mice were bled by cardiac puncture into heparin and gametocytes separated from uninfected erythrocytes on a 48% Nycodenz gradient (27.6% w/v Nycodenz in 5 mM Tris-HCl, pH 7.20, 3 mM KCl, 0.3 mM EDTA) in coelenterazine loading buffer (CLB), containing PBS, 20 mM HEPES, 20 mM Glucose, 4 mM sodium bicarbonate, 1 mM EGTA, 0.1% w/v bovine serum albumin, pH 7.25. Gametocytes were harvested from the interface and washed twice in RPMI 1640 ready for activation of gamete formation. Blood cells from day 5 p.i mice were placed in culture (40 ml RPMI 1640, 8 ml foetal bovine serum, 0.5 ml penicillin and streptomycin; per 0.5 ml blood) for 24 h at 37°C for schizont- (with rotation at 100 rpm) and at

20°C for ookinete production, as described above. Schizonts and ookinetes were purified on 60% and 63% NycoDenz gradients, respectively and harvested from the interface and washed. For 14 dpi oocysts, 20 mosquito midguts were collected and homogenised with PBS in a loosely fitting homogeniser to release sporozoites as described above.

## Transcriptome sequencing and analysis

Parasites (activated gametocytes and ookinetes) were collected from  $\Delta cyc3$  or GFP-expressing lines. Samples were passed through a plasmidipur column to remove host DNA contamination prior to RNA isolation. Total RNA was isolated from purified parasites using an RNeasy purification kit (Qiagen). RNA was vacuum concentrated (SpeedVac) and transported using RNA stable tubes (Biomatrica). Strand-specific mRNA sequencing was performed from total RNA using TruSeq Stranded mRNA Sample Prep Kit LT (Illumina) according to the manufacturer's instructions. Briefly, polyA+ mRNA was purified from total RNA using oligo-dT dyna-bead selection. First strand cDNA was synthesised primed with random oligos followed by second strand synthesis where dUTPs were incorporated to achieve strand-specificity. The cDNA was adapter-ligated and the libraries amplified by PCR. Libraries were sequenced in an Illumina HiSeq machine with paired-end 100bp read chemistry.

RNA-seq read alignments were mapped onto the *P. berghei* ANKA genome (May 2015 release in GeneDB—<http://www.genedb.org/>) using Tophat2 (version 2.0.13) [89] with parameters “—library-type fr-firststrand—no-novel-juncs—r 60”. Transcript abundances (reported as FPKM—fragments per kilobase of exon per million fragments) were quantified and differential expression analysis was performed using Cuffdiff2 version 2.2.1 [90]. Genes with fold change greater than 2 and p-value less than 0.05 were considered as significantly differentially expressed. As a form of independent validation of the differentially expressed genes, transcript abundances were extracted as raw read counts using htseq-count [91] and differential expression analysis performed using DESeq2 [92] in R version 3.2.1. *P. berghei* GO terms (Gene Ontology) were downloaded from GeneDB (<http://www.genedb.org/>; May 2015 release) and gene ontology enrichment analysis was performed for the DEG lists using GOstats R package [93]. All analyses and visualizations were done with R packages—*cummeRbund* [94] and *ggplot2* [95].

## Quantitative RT-PCR

Total RNA was isolated from purified parasites using an RNeasy purification kit (Qiagen). For qRT-PCR, cDNA was synthesised using an RNA-to-cDNA kit (Applied Biosystems) allowing quantification from 250 ng of total RNA. qRT-PCR reactions consisted of 2  $\mu$ l cDNA, 5  $\mu$ l SYBR green fast master mix (Applied Biosystems), 0.5  $\mu$ l (500 nM) each of the forward and reverse primers, and 2  $\mu$ l DEPC-treated water. Where possible, one of the primer pairs was placed over an intron, primers had melting temperatures of 60–62°C and together amplified a region 70–200 bp long. Analysis was conducted using an Applied Biosystems 7500 fast machine with the following cycling conditions: 95°C for 20 sec followed by 40 cycles of 95°C for 3 sec; 60°C for 30 sec. Wild-type expression was determined using the Pfaffl method [96]. Relative quantification in the mutant line was normalised against wild-type expression using the  $\Delta\Delta C_t$  method. Both methods used *hsp70* (and *arginine-tRNA synthetase* for wild-type expression) as a reference gene to provide a baseline of transcription levels between replicates to allow normalization of the data [29]. Three biological replicates were used for each stage (each with two technical replicates). See S1 Table for a full list of the primers used for qRT-PCR. Statistical analyses were performed using Excel and GraphPad Prism (GraphPad Software), with graphs showing normalised expression in  $\Delta cyc3$  compared to a transcription baseline derived from WT. For relative gene expression, a Student's unpaired *t*-test was used.

For RNA-seq and qRT-PCR comparison, we used  $\geq 30$  genes at each stage and used GraphPad Prism (GraphPad Software) to calculate fit and coefficient of determination.

## Yeast experiments

Standard protocols of handling *Schizosaccharomyces pombe* and *Saccharomyces cerevisiae* were followed [97,98]. For yeast complementation experiments, the triple-*cln* mutant (*cln1Δ cln2Δ cln3Δ TRP::GAL1-CLN3 ade1 leu2-3 his2 trp1-1 ura3Δ bar1Δ pep4Δ::LEU2*) or *cdc13 ts* mutant strain (*h- cdc13-117 leu1-32*) was used.

## Deconvolution microscopy

High resolution live cell imaging was performed using an Olympus-based Delta Vision Elite work station fitted with a 100x objective (numerical NA 1.4, oil). Post-acquisition analysis was carried out using Applied Precision software. Images presented are 2D projections of deconvolved Z-stacks of 0.3  $\mu\text{m}$  optical sections.

## Ookinete motility assay

The ookinete motility assay was performed as previously described [99]. Twenty five microliters of the ookinete cultures were added to an equal volume of Matrigel (BD) on ice, mixed thoroughly, added to a slide, covered with a Vaseline-rimmed cover slip, and sealed with nail varnish. The Matrigel was then allowed to set at room temperature for at least 30 minutes. After identifying a field containing ookinetes, time-lapse videos (1 frame every 5 sec, for 10 min) were taken of ookinetes using the differential interference contrast (DIC) settings with a 63 $\times$  objective lens on a Zeiss AxioImager M2 microscope fitted with an AxioCam ICc1 digital camera controlled by the Axiovision (Zeiss) software package. Speed of motility of individual ookinetes was measured by multiplying the number of body lengths moved by the length of the ookinete during the 10 min video, divided by 10. Multiple independent slides and cultures were used for each parasite line.

## Ookinete nuclear DNA content measurement

The nuclear content of the  $\Delta\text{cyc}3$  ookinete was measured by the formula as previously described [58]. Briefly, to measure nuclear DNA content of microgametocytes, digital images of Hoechst-stained fixed or unfixed cells were obtained using a Zeiss AxioImager M2 microscope fitted with an AxioCam ICc1 digital camera and analysed using ImageJ software version 1.33u (National Institutes of Health, USA). The relative nuclear fluorescence intensity was determined with the following formula:  $\text{Area (pixel)} \times (\text{average intensity (relative units)} - \text{average background intensity (relative units)})$ . The nuclear fluorescence intensity was standardized to the haploid DNA content by measuring the fluorescence intensity of ring-stage parasites in parallel on the same slide and with the same microscope and camera settings.

## Supporting Information

**S1 Fig. Phylogenetic analysis of cyclins.** A maximum likelihood protein phylogeny comparing apicomplexan cyclins to sequences from human, *Schizosaccharomyces pombe*, and *Trypanosoma brucei*. Select *Arabidopsis* cyclins and Pho80 from *Saccharomyces cerevisiae* have been included for clarity of protein families. A consensus tree from 100 bootstrap replicates based on 270 alignable positions is shown with topology support at nodes. Protein domain architectures were predicted from the models in Pfam27 with e-value  $\leq 0.001$ . (TIF)

**S2 Fig. Generation and genotypic analysis of CYC3-GFP parasites.** (A) Schematic representation of the endogenous *cyc3* locus, the GFP-tagging construct and the recombined *cyc3* locus following single cross-over recombination. Following recombination, the *cyc3* locus contains the tagged copy and the original *cyc3* CDS lacking all but 332 bp of upstream region, which is unlikely to sufficient for transcription. Arrows 1 and 2 indicate PCR primers used to confirm successful integration in the *cyc3* locus following recombination. (B) Integration PCR of the *cyc3* locus in wild type and CYC3-GFP parasites using primers IntT89 and ol492. Integration of *cyc3* with *gfp* gives a band of 1.2 kb. (C) Pulse Field Gel Electrophoresis (PFGE) using a *pbdfhr* 3'UTR probe. The probe recognises the endogenous *dhfr* locus on chromosome 7 and the recombined *cyc3* locus on chromosome 12. (D) Southern blot analysis of WT and *cyc3* parasite genomic DNA following BsmI digestion. A probe specific for the fragment homologous to the *P. berghei* genomic *cyc3* sequence cloned in the p277 vector bound to a 5.5 kb band in WT and to a 12 kb band in  $\Delta$ *cyc3* parasites. (E) Western blot of CYC3-GFP (54 kDa) and WT-GFP (29 kDa) protein to illustrate CYC3-GFP concentration in three different parasite stages. Total protein concentration for CYC3-GFP samples was normalised across all three samples and controlled by a Coomassie gel (see below the western blot). WT-GFP is shown as a control. Sch: schizont, AG: activated gametocytes, Ook: Ookinetes. (F) Total number of oocysts per infected mosquito at 14 dpi for CYC3-GFP and WT lines. Bar is the mean  $\pm$  SEM.  $n = 2$  independent experiments (15 mosquitoes for each)  $p > 0.1$ . As the tagged line is not a clonal population, in the CYC3-GFP parasite line 86% of oocysts were expressing GFP. The rest of the oocysts are a WT population (not expressing GFP). (G) Individual CYC3-GFP and WT oocyst diameters measured in  $\mu\text{m}$  at 14 dpi  $p < 0.001$ . (TIF)

**S3 Fig. Generation and genotypic analysis of  $\Delta$ *cyc3* parasites.** (A) Schematic representation of the endogenous *cyc3* locus, the targeting knock out construct and the recombined *cyc3* locus following double homologous cross-over recombination. Arrows 1 and 2 indicate PCR primers used to confirm successful integration in the *cyc3* locus following recombination and arrows 3 and 4 indicate PCR primers used to show deletion of the *cyc3* gene. (B) Integration PCR of the *cyc3* locus in WT and  $\Delta$ *cyc3* cl.1 and cl.3 parasites using primers INT N45 and ol248. Integration of the targeting construct gives a band of 0.7 kb. Presence of the gene gives a band of 0.2 kb. (C) Southern blot analysis of WT, *cyc3* cl.1 and *cyc3* cl.3 parasite genomic DNA following HindIII digestion. A probe specific for the *cyc3* 3'UTR bound to a 3.7 kb band in WT and to a 7.6 kb band in  $\Delta$ *cyc3* parasites. (D) Pulse Field Gel Electrophoresis (PFGE) using a *pbdfhr* 3'UTR probe. The probe recognises the endogenous *dhfr* locus on chromosome 7, the *gfp* cassette integrated in the 230p locus of the GFP-transgenic parasites used for transfection (chromosome 4) and the recombined *cyc3* locus on chromosome 12. (TIF)

**S4 Fig. Sporozoite numbers in WT and  $\Delta$ *cyc3* parasite lines and  $\Delta$ *cyc3* ookinetes show no observable phenotypes.** (A) Total number of sporozoites per mosquito from 21 dpi salivary glands for  $\Delta$ *cyc3* and WT lines. Three independent experiments are described,  $n = 20$  mosquitoes for each replicate. (B) Table of mosquito numbers for  $\Delta$ *cyc3* and WT lines. Bite back data are presented as day in which blood stage parasites are observed. dpi = days post infection. (C) Low power ultrastructural images of WT (i) and  $\Delta$ *cyc3* (ii) ookinetes. N—nucleus. M—micronemes. Bars represent 1  $\mu\text{m}$ . (D) Graph representing the DNA content of  $\Delta$ *cyc3* ookinetes compared to WT. (E) Graph representing the motility of  $\Delta$ *cyc3* ookinetes compared to WT. (TIF)

**S5 Fig. Complementation of cyclin in yeast.** (A) *Plasmodium cyc3* cannot complement the triple *cln* (G1 cyclin) mutant of the budding yeast *Saccharomyces cerevisiae*. The triple-*cln* mutant *cln1 cln2 cln3* is lethal (+Glucose, empty vector), but it can be rescued by GAL-*CLN3* (+Galactose). *Plasmodium cyc3*, *CLN2* or empty vector was expressed under the control of the methionine-repressible MET3 promoter. In the absence of methionine (promoter ON), *Plasmodium cyc3* (MET3-Pb\_ycyc3) was unable to rescue and form any colony whereas MET3-*CLN2* rescued the triple *cln* mutant and these cells grew normally. (B) *Plasmodium cyc3* cannot complement the temperature-sensitive (ts) defect of a *cdc13-117* allele (B-type cyclin) of the fission yeast *Schizosaccharomyces pombe*. The ts *cdc13-117* mutant strains expressing the indicated plasmids were grown on the minimal medium plates in the absence of thiamine for 3 days at the restrictive temperature (36°C) or the permissive temperature (25°C). Cyclins were expressed from the *nmt1* medium-strength promoter (pREP41) or low-strength promoter (pREP81). Although *S. pombe cdc13*<sup>+</sup> rescued the temperature sensitivity (36°C), neither Pk epitope-tagged nor MH (c-myc and His6) tagged *Pbcyc3* rescued. At the permissive temperature (25°C), all the strains grew normally. (TIF)

**S6 Fig. Transcript analysis.** (A) Strand-specific RNAseq reads aligned onto *Plasmodium berghei* genome, as visualized using Artemis. *cyc3* gene is expressed in the wild types as shown by RNAseq reads in the reverse (-ve) strand, while a major portion of the gene is deleted in the knockouts as shown by the absence of RNAseq reads (area shaded in red). (B) Multidimensional scaling of gene expression values for WT and  $\Delta$ *cyc3* RNA-seq samples shows tight correlation among individual replicates within each sample group. (C) Heatmaps for cell cycle, inner membrane complex and apiAP2 transcription factor gene clusters based on their log<sub>2</sub> fold change in  $\Delta$ *cyc3* activated gametocytes (inner circular track) and  $\Delta$ *cyc3* ookinetes (outer circular track) relative to WT. Functional groups were inferred from annotations available in GeneDB (<http://www.genedb.org/>). Genes that were found significantly misregulated are shown in bold and those validated by qRT-PCR are shown in red. Full gene list and functional clusters are shown in S3 Table. (D) GO term enrichment analysis of *cyc3* activated gametocytes and ookinetes. The size of the dot is proportional to the level of significance and the color intensity represents the fold enrichment of enriched terms in biological process (green), molecular function (purple) and cellular component (pink). (TIF)

**S1 Table. Oligonucleotides used in this study.**  
(XLSX)

**S2 Table. List of differentially expressed genes (FDR-corrected p value < 0.05) between  $\Delta$ *cyc3* and WT activated gametocytes and ookinetes.**  
(XLSX)

**S3 Table. RNA-seq data and functional clusters used to generate the heat maps.**  
(XLSX)

## Acknowledgments

We are grateful to Julie Rodgers, Jessica Stock, Alyaa M. Abdel-Haleem and Dr. Benoit Poulin for their technical advice and assistance. We also thank Dr. Rob de Bruin for providing yeast strains and plasmids.



## Author Contributions

Conceived and designed the experiments: BW RT. Performed the experiments: RT MR RJW AR DJPF MLK LB NJ ZR DB DSG SPW HY BW. Analyzed the data: RT BW RJW MR AAH AP DJPF SPW HY AR DSG LB. Contributed reagents/materials/analysis tools: DJPF AP HY AAH BW RT. Wrote the paper: MR RJW BW RT. Performed the Functional and GFP tagging experiments: RT MR RJW LB MLK DB DSG SPW. Phylogenetics analysis: APD BW. RNAseq experiment: AR ZR AP. QPCR analysis: NJ MR RJW. Yeast complementation experiment: HY. Electron microscopy experiment: DJPF.

## References

1. Chang L, Zhang Z, Yang J, McLaughlin SH, Barford D (2014) Molecular architecture and mechanism of the anaphase-promoting complex. *Nature* 513: 388–393. doi: [10.1038/nature13543](https://doi.org/10.1038/nature13543) PMID: [25043029](https://pubmed.ncbi.nlm.nih.gov/25043029/)
2. Cross F, Buchler N, Skotheim J (2011) Evolution of networks and sequences in eukaryotic cell cycle control. *Philos Trans R Soc Lond B Biol Sci* 366: 3532–3544. doi: [10.1098/rstb.2011.0078](https://doi.org/10.1098/rstb.2011.0078) PMID: [22084380](https://pubmed.ncbi.nlm.nih.gov/22084380/)
3. Fisher D, Krasinska L., Coudreuse D., and Novák B. (2012) Phosphorylation network dynamics in the control of cell cycle transitions. *J Cell Sci* 125: 4703–4711. doi: [10.1242/jcs.106351](https://doi.org/10.1242/jcs.106351) PMID: [23223895](https://pubmed.ncbi.nlm.nih.gov/23223895/)
4. Harashima H, Dissmeyer N, Schnittger A (2013) Cell cycle control across the eukaryotic kingdom. *Trends Cell Biol* 23: 345–356. doi: [10.1016/j.tcb.2013.03.002](https://doi.org/10.1016/j.tcb.2013.03.002) PMID: [23566594](https://pubmed.ncbi.nlm.nih.gov/23566594/)
5. Morgan DO (1997) Cyclin-dependent kinases: engines, clocks, and microprocessors. *Annu Rev Cell Dev Biol* 13: 261–291. PMID: [9442875](https://pubmed.ncbi.nlm.nih.gov/9442875/)
6. Hochegger H, Takeda S, Hunt T (2008) Cyclin-dependent kinases and cell-cycle transitions: does one fit all? *Nat Rev Mol Cell Biol* 9: 910–916. doi: [10.1038/nrm2510](https://doi.org/10.1038/nrm2510) PMID: [18813291](https://pubmed.ncbi.nlm.nih.gov/18813291/)
7. Nigg EA (2001) Mitotic kinases as regulators of cell division and its checkpoints. *Nat Rev Mol Cell Biol* 2: 21–32. PMID: [11413462](https://pubmed.ncbi.nlm.nih.gov/11413462/)
8. Glotzer M, Murray AW, Kirschner MW (1991) Cyclin is degraded by the ubiquitin pathway. *Nature* 349: 132–138. PMID: [1846030](https://pubmed.ncbi.nlm.nih.gov/1846030/)
9. Murray AW (2004) Recycling the cell cycle: cyclins revisited. *Cell* 116: 221–234. PMID: [14744433](https://pubmed.ncbi.nlm.nih.gov/14744433/)
10. Bloom J, Cross F (2007) Multiple levels of cyclin specificity in cell-cycle control. *Nat Rev Mol Cell Biol* 8: 149–160. PMID: [17245415](https://pubmed.ncbi.nlm.nih.gov/17245415/)
11. Loyer P, Trembley JH, Katona R, Kidd VJ, Lahti JM (2005) Role of CDK/cyclin complexes in transcription and RNA splicing. *Cell Signal* 17: 1033–1051. PMID: [15935619](https://pubmed.ncbi.nlm.nih.gov/15935619/)
12. Cao L, Chen F, Yang X, Xu W, Xie J, et al. (2014) Phylogenetic analysis of CDK and cyclin proteins in premetazoan lineages. *BMC Evolutionary Biology* 14: 10. doi: [10.1186/1471-2148-14-10](https://doi.org/10.1186/1471-2148-14-10) PMID: [24433236](https://pubmed.ncbi.nlm.nih.gov/24433236/)
13. Ma Z, Wu Y., Jin J., Yan J., Kuang S., Zhou M., et al. (2013) Phylogenetic analysis reveals the evolution and diversification of cyclins in eukaryotes. *Mol Phylogenet Evol* 66: 1002–1010. doi: [10.1016/j.ympev.2012.12.007](https://doi.org/10.1016/j.ympev.2012.12.007) PMID: [23261709](https://pubmed.ncbi.nlm.nih.gov/23261709/)
14. Hunt T, Luca FC, Ruderman JV (1992) The requirements for protein synthesis and degradation, and the control of destruction of cyclins A and B in the meiotic and mitotic cell cycles of the clam embryo. *The Journal of Cell Biology* 116: 707–724. PMID: [1530948](https://pubmed.ncbi.nlm.nih.gov/1530948/)
15. Vermeulen K, Van Bockstaele DR, Berneman ZN (2003) The cell cycle: a review of regulation, deregulation and therapeutic targets in cancer. *Cell Prolif* 36: 131–149. PMID: [12814430](https://pubmed.ncbi.nlm.nih.gov/12814430/)
16. Carroll AS, and O'Shea E.K. (2002) Pho85 and signaling environmental conditions. *Trends Biochem Sci* 27: 87–93. PMID: [11852246](https://pubmed.ncbi.nlm.nih.gov/11852246/)
17. Torres Acosta JA, de Almeida Engler J, Raes J, Magyar Z, De Groot R, et al. (2004) Molecular characterization of *Arabidopsis* PHO80-like proteins, a novel class of CDKA<sub>1</sub>-interacting cyclins. *Cell Mol Life Sci* 61: 1485–1497. PMID: [15197472](https://pubmed.ncbi.nlm.nih.gov/15197472/)
18. Peng L, Skylar A., Chang P.L., Bisova K., and Wu X. (2014) CYCP2;1 integrates genetic and nutritional information to promote meristem cell division in *Arabidopsis*. *Dev Biol* 393: 160–170. doi: [10.1016/j.ydbio.2014.06.008](https://doi.org/10.1016/j.ydbio.2014.06.008) PMID: [24951878](https://pubmed.ncbi.nlm.nih.gov/24951878/)
19. Van Hellemond JJ, Neuville P, Schwarz RT, Matthews KR, Mottram JC (2000) Isolation of *Trypanosoma brucei* CYC2 and CYC3 cyclin genes by rescue of a yeast G(1) cyclin mutant. Functional characterization of CYC2. *J Biol Chem* 275: 8315–8323. PMID: [10722661](https://pubmed.ncbi.nlm.nih.gov/10722661/)

20. Toh-E A, Shimauchi T (1986) Cloning and sequencing of the PHO80 gene and CEN15 of *Saccharomyces cerevisiae*. *Yeast* 2: 129–139. PMID: [3333302](#)
21. Arnot DE, Ronander E, Bengtsson DC (2011) The progression of the intra-erythrocytic cell cycle of *Plasmodium falciparum* and the role of the centriolar plaques in asynchronous mitotic division during schizogony. *International Journal for Parasitology* 41: 71–80. doi: [10.1016/j.ijpara.2010.07.012](#) PMID: [20816844](#)
22. Sinden RE (1991) Asexual blood stages of malaria modulate gametocyte infectivity to the mosquito vector—possible implications for control strategies. *Parasitology* 103 Pt 2: 191–196. PMID: [1684037](#)
23. Sinden RE (1991) Mitosis and meiosis in malarial parasites. *Acta Leiden* 60: 19–27. PMID: [1820709](#)
24. Aly AS, Vaughan AM, Kappe SH (2009) Malaria parasite development in the mosquito and infection of the mammalian host. *Annu Rev Microbiol* 63: 195–221. doi: [10.1146/annurev.micro.091208.073403](#) PMID: [19575563](#)
25. Sinden RE, Canning EU, Bray RS, Smalley ME (1978) Gametocyte and gamete development in *Plasmodium falciparum*. *Proc R Soc Lond B Biol Sci* 201: 375–399. PMID: [27809](#)
26. Sinden RE, Talman A, Marques SR, Wass MN, Sternberg MJ (2010) The flagellum in malarial parasites. *Curr Opin Microbiol* 13: 491–500. doi: [10.1016/j.mib.2010.05.016](#) PMID: [20566299](#)
27. Arnot DE, Gull K (1998) The *Plasmodium* cell-cycle: facts and questions. *Ann Trop Med Parasitol* 92: 361–365. PMID: [9683889](#)
28. Edgar BA, Orr-Weaver TL (2001) Endoreplication cell cycles: more for less. *Cell* 105: 297–306. PMID: [11348589](#)
29. Guttery DS, Ferguson DJ, Poulin B, Xu Z, Straschil U, et al. (2012) A putative homologue of CDC20/CDH1 in the malaria parasite is essential for male gamete development. *PLoS Pathog* 8: e1002554. doi: [10.1371/journal.ppat.1002554](#) PMID: [22383885](#)
30. Guttery DS, Poulin B, Ramaprasad A, Wall RJ, Ferguson DJ, et al. (2014) Genome-wide functional analysis of *Plasmodium* protein phosphatases reveals key regulators of parasite development and differentiation. *Cell Host Microbe* 16: 128–140. doi: [10.1016/j.chom.2014.05.020](#) PMID: [25011111](#)
31. Tewari R, Straschil U, Bateman A, Bohme U, Cherevach I, et al. (2010) The systematic functional analysis of *Plasmodium* protein kinases identifies essential regulators of mosquito transmission. *Cell Host Microbe* 8: 377–387. doi: [10.1016/j.chom.2010.09.006](#) PMID: [20951971](#)
32. Solyakov L, Halbert J, Alam MM, Semblat JP, Dorin-Semblat D, et al. (2011) Global kinomic and phospho-proteomic analyses of the human malaria parasite *Plasmodium falciparum*. *Nat Commun* 2: 565. doi: [10.1038/ncomms1558](#) PMID: [22127061](#)
33. Reiningger L, Wilkes JM, Bourgade H, Miranda-Saavedra D, Doerig C (2011) An essential Aurora-related kinase transiently associates with spindle pole bodies during *Plasmodium falciparum* erythrocytic schizogony. *Molecular Microbiology* 79: 205–221. doi: [10.1111/j.1365-2958.2010.07442.x](#) PMID: [21166904](#)
34. Le Roch K, Sestier C, Dorin D, Waters N, Kappes B, et al. (2000) Activation of a *Plasmodium falciparum* cdc2-related kinase by heterologous p25 and cyclin H. Functional characterization of a *P. falciparum* cyclin homologue. *J Biol Chem* 275: 8952–8958. PMID: [10722743](#)
35. Merckx A, Le Roch K, Nivez MP, Dorin D, Alano P, et al. (2003) Identification and initial characterization of three novel cyclin-related proteins of the human malaria parasite *Plasmodium falciparum*. *J Biol Chem* 278: 39839–39850. PMID: [12869562](#)
36. Kaneko I, Iwanaga S., Kato T., Kobayashi I., Yuda M. (2015) Genome-Wide Identification of the Target Genes of AP2-O, a *Plasmodium* AP2-Family Transcription Factor. *PLoS Pathog* 11: e1004905. doi: [10.1371/journal.ppat.1004905](#) PMID: [26018192](#)
37. Fisher DL, Nurse P (1996) A single fission yeast mitotic cyclin B p34cdc2 kinase promotes both S-phase and mitosis in the absence of G1 cyclins. *EMBO J* 15: 850–860. PMID: [8631306](#)
38. Fisher RP, and Morgan D.O. (1994) A novel cyclin associates with MO15/CDK7 to form the CDK-activating kinase. *Cell* 78: 713–724. PMID: [8069918](#)
39. Feaver WJ, Svejstrup J.Q., Henry N.L., and Kornberg R.D. (1994) Relationship of CDK-activating kinase and RNA polymerase II CTD kinase TFIIF/TFIIK. *Cell* 79: 1103–1109. PMID: [8001136](#)
40. Roy R, Adamczewski J.P., Seroz T., Vermeulen W., Tassan J.P., Schaeffer L., et al. (1994) The MO15 cell cycle kinase is associated with the TFIIF transcription-DNA repair factor. *Cell* 79: 1093–1101. PMID: [8001135](#)
41. Drogat J, Migeot V., Mommaerts E., Mullier C., Dieu M., van Bakel H., et al. (2012) Cdk11-cyclinL controls the assembly of the RNA polymerase II mediator complex. *Cell Rep* 2: 1068–1076. doi: [10.1016/j.celrep.2012.09.027](#) PMID: [23122962](#)

42. Otto TD, Bohme U, Jackson AP, Hunt M, Franke-Fayard B, et al. (2014) A comprehensive evaluation of rodent malaria parasite genomes and gene expression. *BMC Biol* 12: 86. doi: [10.1186/s12915-014-0086-0](https://doi.org/10.1186/s12915-014-0086-0) PMID: [25359557](https://pubmed.ncbi.nlm.nih.gov/25359557/)
43. Lopez-Barragan MJ, Lemieux J, Quinones M, Williamson KC, Molina-Cruz A, et al. (2011) Directional gene expression and antisense transcripts in sexual and asexual stages of *Plasmodium falciparum*. *BMC Genomics* 12: 587. doi: [10.1186/1471-2164-12-587](https://doi.org/10.1186/1471-2164-12-587) PMID: [22129310](https://pubmed.ncbi.nlm.nih.gov/22129310/)
44. Janse CJ, Franke-Fayard B, Mair GR, Ramesar J, Thiel C, et al. (2006) High efficiency transfection of *Plasmodium berghei* facilitates novel selection procedures. *Mol Biochem Parasitol* 145: 60–70. PMID: [16242190](https://pubmed.ncbi.nlm.nih.gov/16242190/)
45. Liu Y, Tewari R, Ning J, Blagborough AM, Garbom S, et al. (2008) The conserved plant sterility gene HAP2 functions after attachment of fusogenic membranes in *Chlamydomonas* and *Plasmodium* gametes. *Genes Dev* 22: 1051–1068. doi: [10.1101/gad.1656508](https://doi.org/10.1101/gad.1656508) PMID: [18367645](https://pubmed.ncbi.nlm.nih.gov/18367645/)
46. Mair GR, Braks JA, Garver LS, Wiegant JC, Hall N, et al. (2006) Regulation of sexual development of *Plasmodium* by translational repression. *Science* 313: 667–669. PMID: [16888139](https://pubmed.ncbi.nlm.nih.gov/16888139/)
47. Reininger L, Billker O, Tewari R, Mukhopadhyay A, Fennell C, et al. (2005) A NIMA-related protein kinase is essential for completion of the sexual cycle of malaria parasites. *J Biol Chem* 280: 31957–31964. PMID: [15970588](https://pubmed.ncbi.nlm.nih.gov/15970588/)
48. van Dijk MR, Janse CJ, Thompson J, Waters AP, Braks JA, et al. (2001) A central role for P48/45 in malaria parasite male gamete fertility. *Cell* 104: 153–164. PMID: [11163248](https://pubmed.ncbi.nlm.nih.gov/11163248/)
49. Doerig C, Billker O., Pratt D., and Endicott J. (2005) Protein kinases as targets for antimalarial intervention: Kinomics, structure-based design, transmission-blockade, and targeting host cell enzymes. *Biochim Biophys Acta* 1754: 132–150. PMID: [16271522](https://pubmed.ncbi.nlm.nih.gov/16271522/)
50. Dorin-Semblat D, Bottrill AR., Solyakov L., Tobin A., Doerig C. (2013) Experimental tools for the study of protein phosphorylation in *Plasmodium*. *Methods Mol Biol* 923: 241–257.
51. Painter HJ, Campbell TL, Llinás M (2011) The Apicomplexan AP2 family: Integral factors regulating *Plasmodium* development. *Molecular and Biochemical Parasitology* 176: 1–7. doi: [10.1016/j.molbiopara.2010.11.014](https://doi.org/10.1016/j.molbiopara.2010.11.014) PMID: [21126543](https://pubmed.ncbi.nlm.nih.gov/21126543/)
52. Yuda M, Iwanaga S, Shigenobu S, Mair GR, Janse CJ, et al. (2009) Identification of a transcription factor in the mosquito-invasive stage of malaria parasites. *Molecular Microbiology* 71: 1402–1414. doi: [10.1111/j.1365-2958.2009.06609.x](https://doi.org/10.1111/j.1365-2958.2009.06609.x) PMID: [19220746](https://pubmed.ncbi.nlm.nih.gov/19220746/)
53. Yuda M, Iwanaga S, Shigenobu S, Kato T, Kaneko I (2010) Transcription factor AP2-Sp and its target genes in malarial sporozoites. *Molecular Microbiology* 75: 854–863. doi: [10.1111/j.1365-2958.2009.07005.x](https://doi.org/10.1111/j.1365-2958.2009.07005.x) PMID: [20025671](https://pubmed.ncbi.nlm.nih.gov/20025671/)
54. Iwanaga S, Kaneko I, Kato T, Yuda M (2012) Identification of an AP2-family Protein That Is Critical for Malaria Liver Stage Development. *PLoS ONE* 7: e47557. doi: [10.1371/journal.pone.0047557](https://doi.org/10.1371/journal.pone.0047557) PMID: [23144823](https://pubmed.ncbi.nlm.nih.gov/23144823/)
55. Sinha A, Hughes KR, Modrzynska KK, Otto TD, Pfander C, et al. (2014) A cascade of DNA-binding proteins for sexual commitment and development in *Plasmodium*. *Nature* 507: 253–257. doi: [10.1038/nature12970](https://doi.org/10.1038/nature12970) PMID: [24572359](https://pubmed.ncbi.nlm.nih.gov/24572359/)
56. Woo YH, Ansari H, Otto TD, Klinger CM, Kolisko M, et al. (2015) Chromerid genomes reveal the evolutionary path from photosynthetic algae to obligate intracellular parasites. *eLife* 4.
57. Billker O, Dechamps S, Tewari R, Wenig G, Franke-Fayard B, et al. (2004) Calcium and a calcium-dependent protein kinase regulate gamete formation and mosquito transmission in a malaria parasite. *Cell* 117: 503–514. PMID: [15137943](https://pubmed.ncbi.nlm.nih.gov/15137943/)
58. Tewari R, Dorin D, Moon R, Doerig C, Billker O (2005) An atypical mitogen-activated protein kinase controls cytokinesis and flagellar motility during male gamete formation in a malaria parasite. *Mol Microbiol* 58: 1253–1263. PMID: [16313614](https://pubmed.ncbi.nlm.nih.gov/16313614/)
59. Reininger L, Tewari R, Fennell C, Holland Z, Goldring D, et al. (2009) An essential role for the *Plasmodium* Nek-2 Nima-related protein kinase in the sexual development of malaria parasites. *J Biol Chem* 284: 20858–20868. doi: [10.1074/jbc.M109.017988](https://doi.org/10.1074/jbc.M109.017988) PMID: [19491095](https://pubmed.ncbi.nlm.nih.gov/19491095/)
60. Angrisano F, Tan YH, Sturm A, McFadden GI, Baum J (2012) Malaria parasite colonisation of the mosquito midgut—placing the *Plasmodium* ookinete centre stage. *Int J Parasitol* 42: 519–527. doi: [10.1016/j.ijpara.2012.02.004](https://doi.org/10.1016/j.ijpara.2012.02.004) PMID: [22406332](https://pubmed.ncbi.nlm.nih.gov/22406332/)
61. Bergman LW, Kaiser K, Fujioka H, Coppens I, Daly TM, et al. (2003) Myosin A tail domain interacting protein (MTIP) localizes to the inner membrane complex of *Plasmodium* sporozoites. *J Cell Sci* 116: 39–49. PMID: [12456714](https://pubmed.ncbi.nlm.nih.gov/12456714/)
62. Srinivasan P, Fujioka H, Jacobs-Lorena M (2008) *PbCap380*, a novel oocyst capsule protein, is essential for malaria parasite survival in the mosquito. *Cellular Microbiology* 10: 1304–1312. doi: [10.1111/j.1462-5822.2008.01127.x](https://doi.org/10.1111/j.1462-5822.2008.01127.x) PMID: [18248630](https://pubmed.ncbi.nlm.nih.gov/18248630/)

63. Menard R, Sultan AA, Cortes C, Altszuler R, van Dijk MR, et al. (1997) Circumsporozoite protein is required for development of malaria sporozoites in mosquitoes. *Nature* 385: 336–340. PMID: [9002517](#)
64. Minshull J, Pines J, Golsteyn R, Standart N, Mackie S, et al. (1989) The role of cyclin synthesis, modification and destruction in the control of cell division. *J Cell Sci Suppl* 12: 77–97. PMID: [2534558](#)
65. Li Z, Wang CC (2003) A PHO80-like cyclin and a B-type cyclin control the cell cycle of the procyclic form of *Trypanosoma brucei*. *J Biol Chem* 278: 20652–20658. PMID: [12665514](#)
66. Liu Y, Hu H, Li Z (2013) The cooperative roles of PHO80-like cyclins in regulating the G1/S transition and posterior cytoskeletal morphogenesis in *Trypanosoma brucei*. *Mol Microbiol* 90: 130–146. doi: [10.1111/mmi.12352](#) PMID: [23909752](#)
67. Hammarton TC, Engstler M., and Mottram J.C. (2004) The *Trypanosoma brucei* cyclin, CYC2, is required for cell cycle progression through G1 phase and for maintenance of procyclic form cell morphology. *J Biol Chem* 279: 24757–24764. PMID: [15039435](#)
68. Lew DJ, Dulić V., and Reed S.I. (1991) Isolation of three novel human cyclins by rescue of G1 cyclin (Cln) function in yeast. *Cell* 66: 1197–1206. PMID: [1833066](#)
69. Ward P, Equinet L., Packer J., and Doerig C. (2004) Protein kinases of the human malaria parasite *Plasmodium falciparum*: the kinome of a divergent eukaryote. *BMC Genomics* 5: 79. PMID: [15479470](#)
70. Waters NC, Woodard C.L., and Prigge S.T. (2000) Cyclin H activation and drug susceptibility of the *Pfmrk* cyclin dependent protein kinase from *Plasmodium falciparum*. *Mol Biochem Parasitol* 107: 45–55. PMID: [10717301](#)
71. Chen Y, Jirage D, Caridha D, Kathcart AK, Cortes EA, et al. (2006) Identification of an effector protein and gain-of-function mutants that activate *Pfmrk*, a malarial cyclin-dependent protein kinase. *Molecular and Biochemical Parasitology* 149: 48–57. PMID: [16737745](#)
72. Gourguechon S, Savich JM, Wang CC (2007) The multiple roles of cyclin E1 in controlling cell cycle progression and cellular morphology of *Trypanosoma brucei*. *J Mol Biol* 368: 939–950. PMID: [17376478](#)
73. Ning J, Otto TD, Pfander C, Schwach F, Brochet M, et al. (2013) Comparative genomics in *Chlamydomonas* and *Plasmodium* identifies an ancient nuclear envelope protein family essential for sexual reproduction in protists, fungi, plants, and vertebrates. *Genes Dev* 27: 1198–1215. doi: [10.1101/gad.212746.112](#) PMID: [23699412](#)
74. Mlambo G, Coppens I, Kumar N (2012) Aberrant sporogonic development of Dmc1 (a meiotic recombinase) deficient *Plasmodium berghei* parasites. *PLoS One* 7: e52480. doi: [10.1371/journal.pone.0052480](#) PMID: [23285059](#)
75. Raine JD, Ecker A, Mendoza J, Tewari R, Stanway RR, et al. (2007) Female inheritance of malarial lap genes is essential for mosquito transmission. *PLoS Pathog* 3: e30. PMID: [17335349](#)
76. Ecker A, Bushell ES, Tewari R, Sinden RE (2008) Reverse genetics screen identifies six proteins important for malaria development in the mosquito. *Mol Microbiol* 70: 209–220. doi: [10.1111/j.1365-2958.2008.06407.x](#) PMID: [18761621](#)
77. Bushell ES, Ecker A, Schlegelmilch T, Goulding D, Dougan G, et al. (2009) Paternal effect of the nuclear formin-like protein MISFIT on *Plasmodium* development in the mosquito vector. *PLoS Pathog* 5: e1000539. doi: [10.1371/journal.ppat.1000539](#) PMID: [19662167](#)
78. Hliscs M, Sattler JM, Tempel W, Artz JD, Dong A, et al. (2010) Structure and function of a G-actin sequestering protein with a vital role in malaria oocyst development inside the mosquito vector. *J Biol Chem* 285: 11572–11583. doi: [10.1074/jbc.M109.054916](#) PMID: [20083609](#)
79. Fernandez ML, Engels KK, Bender F, Gassel M, Marhofer RJ, et al. (2012) High-throughput screening with the *Eimeria tenella* CDC2-related kinase2/cyclin complex *EtCRK2/EtCYC3a*. *Microbiology* 158: 2262–2271. doi: [10.1099/mic.0.059428-0](#) PMID: [22723289](#)
80. Ansari A, and Tuteja R. (2012) Genome wide comparative comprehensive analysis of *Plasmodium falciparum* MCM family with human host. *Communicative & Integrative Biology* 5: 607–615.
81. Liu Y, Richards TA, Aves SJ (2009) Ancient diversification of eukaryotic MCM DNA replication proteins. *BMC Evol Biol* 9: 60. doi: [10.1186/1471-2148-9-60](#) PMID: [19292915](#)
82. Kinoshita Y, Johnson EM., Gordon RE., Negri-Bell H., Evans MT., Coolbaugh J., Rosario-Peralta Y., Samet J., Slusser E., Birkenbach MP., Daniel DC. (2008) Colocalization of MCM8 and MCM7 with proteins involved in distinct aspects of DNA replication. *Microsc Res Tech* 71: 288–297. PMID: [18072282](#)
83. Eddy SR (2009) A new generation of homology search tools based on probabilistic inference. *Genome Inform* 23: 205–211. PMID: [20180275](#)
84. Katoh K, Misawa K, Kuma K, Miyata T (2002) MAFFT: a novel method for rapid multiple sequence alignment based on fast Fourier transform. *Nucleic Acids Res* 30: 3059–3066. PMID: [12136088](#)

85. Katoh K, Toh H (2008) Recent developments in the MAFFT multiple sequence alignment program. *Brief Bioinform* 9: 286–298. doi: [10.1093/bib/bbn013](https://doi.org/10.1093/bib/bbn013) PMID: [18372315](https://pubmed.ncbi.nlm.nih.gov/18372315/)
86. Guindon S, Dufayard JF, Lefort V, Anisimova M, Hordijk W, et al. (2010) New algorithms and methods to estimate maximum-likelihood phylogenies: assessing the performance of PhyML 3.0. *Syst Biol* 59: 307–321. doi: [10.1093/sysbio/syq010](https://doi.org/10.1093/sysbio/syq010) PMID: [20525638](https://pubmed.ncbi.nlm.nih.gov/20525638/)
87. Ferguson DJ, Henriquez FL, Kirisits MJ, Muench SP, Prigge ST, et al. (2005) Maternal inheritance and stage-specific variation of the apicoplast in *Toxoplasma gondii* during development in the intermediate and definitive host. *Eukaryot Cell* 4: 814–826. PMID: [15821140](https://pubmed.ncbi.nlm.nih.gov/15821140/)
88. Beetsma AL, van de Wiel TJ, Sauerwein RW, Eling WM (1998) *Plasmodium berghei* ANKA: purification of large numbers of infectious gametocytes. *Exp Parasitol* 88: 69–72. PMID: [9501851](https://pubmed.ncbi.nlm.nih.gov/9501851/)
89. Kim D, Pertea G, Trapnell C, Pimentel H, Kelley R, et al. (2013) TopHat2: accurate alignment of transcriptomes in the presence of insertions, deletions and gene fusions. *Genome Biol* 14: R36. doi: [10.1186/gb-2013-14-4-r36](https://doi.org/10.1186/gb-2013-14-4-r36) PMID: [23618408](https://pubmed.ncbi.nlm.nih.gov/23618408/)
90. Trapnell C, Hendrickson DG, Sauvageau M, Goff L, Rinn JL, et al. (2013) Differential analysis of gene regulation at transcript resolution with RNA-seq. *Nature biotechnology* 31: doi: [10.1038/nbt.2450](https://doi.org/10.1038/nbt.2450) PMID: [23222703](https://pubmed.ncbi.nlm.nih.gov/23222703/)
91. Anders S, Pyl PT, Huber W (2015) HTSeq—a Python framework to work with high-throughput sequencing data. *Bioinformatics* 31: 166–169. doi: [10.1093/bioinformatics/btu638](https://doi.org/10.1093/bioinformatics/btu638) PMID: [25260700](https://pubmed.ncbi.nlm.nih.gov/25260700/)
92. Love MI, Huber W, Anders S (2014) Moderated estimation of fold change and dispersion for RNA-seq data with DESeq2. *Genome Biol* 15: 550. PMID: [25516281](https://pubmed.ncbi.nlm.nih.gov/25516281/)
93. Falcon S, Gentleman R (2007) Using GOstats to test gene lists for GO term association. *Bioinformatics* 23: 257–258. PMID: [17098774](https://pubmed.ncbi.nlm.nih.gov/17098774/)
94. Goff L, Trapnell, C. and Kelley, D. (2013) cummeRbund: Analysis, exploration, manipulation, and visualization of Cufflinks high-throughput sequencing data. R package version 2.10.0.
95. Wickham H (2009) ggplot2: elegant graphics for data analysis. Springer New York.
96. Pfaffl MW (2001) A new mathematical model for relative quantification in real-time RT-PCR. *Nucleic Acids Res* 29: e45. PMID: [11328886](https://pubmed.ncbi.nlm.nih.gov/11328886/)
97. Moreno S, Klar A, Nurse P (1991) Molecular genetic analysis of fission yeast *Schizosaccharomyces pombe*. *Methods Enzymol* 194: 795–823. PMID: [2005825](https://pubmed.ncbi.nlm.nih.gov/2005825/)
98. Guthrie CaF, G. R. (Eds.) (1991) *Guide to Yeast Genetics and Molecular Biology*: Acad. Press, San Diego.
99. Moon RW, Taylor CJ, Bex C, Schepers R, Goulding D, et al. (2009) A cyclic GMP signalling module that regulates gliding motility in a malaria parasite. *PLoS Pathog* 5: e1000599. doi: [10.1371/journal.ppat.1000599](https://doi.org/10.1371/journal.ppat.1000599) PMID: [19779564](https://pubmed.ncbi.nlm.nih.gov/19779564/)